Time-course transcriptomics reveals the impact of Treponema pallidum on microvascular endothelial cell function and phenotype

Sean Waugh, Mara C. Goodyear, Alloysius Gomez, Akash Ranasinghe, Karen V. Lithgow, Reza Falsafi, Robert E. W. Hancock, Amy H. Lee, and Caroline E. Cameron

2025

Original citation:

Waugh, S., Goodyear, M. C., Gomez, A., Ranasinghe, A., Lithgow, K. V., Falsafi, R., Hancock, R. E. W., Lee, A. H., & Cameron, C. E. (2025b). Time-course transcriptomics reveals the impact of Treponema pallidum on microvascular endothelial cell function and phenotype. *Frontiers in Microbiology*, *16*, 1649738. https://doi.org/10.3389/fmicb.2025.1649738

frontiers | Frontiers in Microbiology

TYPE Original Research
PUBLISHED 06 October 2025
DOI 10.3389/fmicb.2025.1649738

OPEN ACCESS

EDITED BY
Monica E. Embers,
Tulane University, United States

REVIEWED BY
Steven J. Norris,
University of Texas Health Science Center at Houston, United States
Petra Pospíšilová,
Masaryk University, Czechia

*CORRESPONDENCE
Caroline E. Cameron
caroc@uvic.ca

RECEIVED 18 June 2025
ACCEPTED 11 September 2025
PUBLISHED 06 October 2025

CITATION
Waugh S, Goodyear MC, Gomez A, Ranasinghe A, Lithgow KV, Falsafi R, Hancock REW, Lee AH and Cameron CE (2025) Time-course transcriptomics reveals the impact of *Treponema pallidum* on microvascular endothelial cell function and phenotype. *Front. Microbiol.* 16:1649738. doi: 10.3389/fmicb.2025.1649738

Time-course transcriptomics reveals the impact of *Treponema pallidum* on microvascular endothelial cell function and phenotype

Sean Waugh[1], Mara C. Goodyear[1], Alloysius Gomez[1], Akash Ranasinghe[1], Karen V. Lithgow[1], Reza Falsafi[2], Robert E. W. Hancock[2], Amy H. Lee[3] and Caroline E. Cameron[1,4]*

[1]Department of Biochemistry and Microbiology, University of Victoria, Victoria, BC, Canada, [2]Department of Microbiology and Immunology, University of British Columbia, Vancouver, BC, Canada, [3]Department of Molecular Biology and Biochemistry, Simon Fraser University, Burnaby, BC, Canada, [4]Department of Medicine, Division of Allergy and Infectious Disease, University of Washington, Seattle, WA, United States

Syphilis, caused by *Treponema pallidum* subsp. *pallidum*, is an urgent global public health threat. Syphilis vaccine development has been impeded by limited understanding of the molecular mechanisms that enable *T. pallidum* to establish and maintain infection. The vascular endothelium is critical for *T. pallidum* attachment, dissemination, and host immune response initiation; however, the molecular details of *T. pallidum*-endothelial interactions are incompletely understood. To enhance understanding, we performed time-course transcriptomic profiling on *T. pallidum*-exposed brain microvascular endothelial cells. These analyses showed *T. pallidum* exposure altered pathways related to extracellular matrix, growth factors, integrins, and Rho GTPases. The induced transcriptional response was consistent with endothelial to mesenchymal transition, a process involved in fetal development and vascular dysfunction. In cells exposed to *T. pallidum*, the primary transcription factor associated with this process (Snail) was increased at both the transcript and protein levels, and microscopy analyses demonstrate F-actin cellular contraction. This study provides a comprehensive understanding of the molecular responses of endothelial cells to *T. pallidum* and identified the host pathways that might cause syphilis disease symptoms, information that could aid in syphilis vaccine design.

KEYWORDS

syphilis, vaccine, transcriptomics, *Treponema pallidum*, endothelial cell, pathogenesis

Highlights

- Exposure of microvascular endothelial cells to *Treponema pallidum* subsp. *pallidum* significantly alters the endothelial cell transcriptome.
- Signaling pathways related to extracellular matrix organization, growth factors, integrins, and Rho GTPases were overrepresented for genes differentially expressed in *T. pallidum*-exposed endothelial cells.

- Exposure to *T. pallidum* induces pathways and factors consistent with endothelial to mesenchymal transition, a host process central to development that may explain the devastating effects of congenital infection.
- *T. pallidum* exposure induces expression of Snail, the main transcription factor associated with the process of endothelial to mesenchymal transition.

Introduction

Infectious syphilis, caused by the sexually transmitted bacterium *Treponema pallidum* subsp. *pallidum*, is a multi-stage infection with a global burden of 49.7 million cases (Chen et al., 2023) and 8 million new infections per year amongst individuals 15–49 years of age (World Health Organization, 2024). The infection is systemic, and persists for an individual's lifetime in the absence of effective antibiotic treatment (LaFond and Lukehart, 2006). The bacterium also causes congenital syphilis, with the number of congenital syphilis cases worldwide estimated at approximately 661,000 resulting in 355,000 adverse birth outcomes per year (Gilmour and Walls, 2023). These figures likely represent an underestimation since an accurate determination of the burden of congenital syphilis worldwide is challenging, due to variations in antenatal screening coverage, access to syphilis testing during pregnancy, and availability and quality of surveillance data. As global syphilis cases have reached a 20-year high (Spiteri et al., 2019; Aho et al., 2022; Chen et al., 2023; CDC, 2024), understanding the molecular basis of the *T. pallidum*-host interaction is crucial for developing biomedical interventions to address the escalating public health burden posed by this pathogen.

Treponema pallidum is a highly invasive pathogen with the ability to disseminate via the bloodstream and cross endothelial, blood–brain, and placental barriers (LaFond and Lukehart, 2006). Interactions between *T. pallidum* and microvascular endothelial cells are central to both *T. pallidum* dissemination via the bloodstream and the establishment of disease manifestations. Previous studies investigating endothelial responses to *T. pallidum* using targeted molecular approaches have provided insights into the cellular consequences of *T. pallidum*-host interactions (Riley et al., 1992; Gao et al., 2019; Lithgow et al., 2020, 2021; Zhang and Wang, 2020). Global proteomics and immune secretomics analyses of *T. pallidum*-exposed human brain microvascular endothelial cells (HBMECs) revealed numerous changes in endothelial cellular signaling pathways, including pathways involved in extracellular matrix (ECM) structural changes, dysregulation of cell death/necroptosis, induction of pro-inflammatory cytokine profiles, and suppression of macrophage/monocyte activating immune responses (Waugh et al., 2023). Multiple prior studies have also investigated the host cytokine response induced during *T. pallidum* infection using clinical samples (Knudsen et al., 2009; Cruz et al., 2012; Kenyon et al., 2017, 2018; Reid et al., 2024).

To expand on these findings and identify host signaling pathways that play a role in syphilis pathogenesis, the current study characterized the transcriptional response of the immortalized cell line HBMEC to *T. pallidum* exposure by time-course transcriptome sequencing (RNA-seq; Figure 1). These analyses reveal significant pathway convergence on endothelial to mesenchymal transition (EndMT), a dynamic process involved in various developmental, physiological, and pathological activities (Piera-Velazquez and Jimenez, 2019; Ciszewski et al., 2021) that contributes to vascular destruction in other infectious diseases, such as SARS-CoV-2 infection (Eapen et al., 2020). These characteristics of EndMT suggest potential relevance to the development of symptoms associated with infectious and congenital syphilis. The systems biology approach pursued in this study provides insight into molecular signaling and cellular transformations occurring in the host that collectively shape the course of *T. pallidum* infection.

Methods

Treponema pallidum growth

Outbred male specific pathogen-free (SPF) New Zealand White rabbits (3.0–3.5 kg, Charles River Laboratories, Ontario, Canada) with nonreactive syphilis serological tests (VDRL and FTA-ABS) were used for *in vivo* propagation of *T. pallidum* subsp. *pallidum* Nichols strain as previously described (Lukehart and Marra, 2007). All rabbits were fed antibiotic-free food and water, and were housed at 18–20 °C. Animal studies were approved by the local institutional review board under protocol 2020–024 and were conducted in strict accordance with standard accepted principles as set forth by the Canadian Council on Animal Care (CCAC), National Institutes of

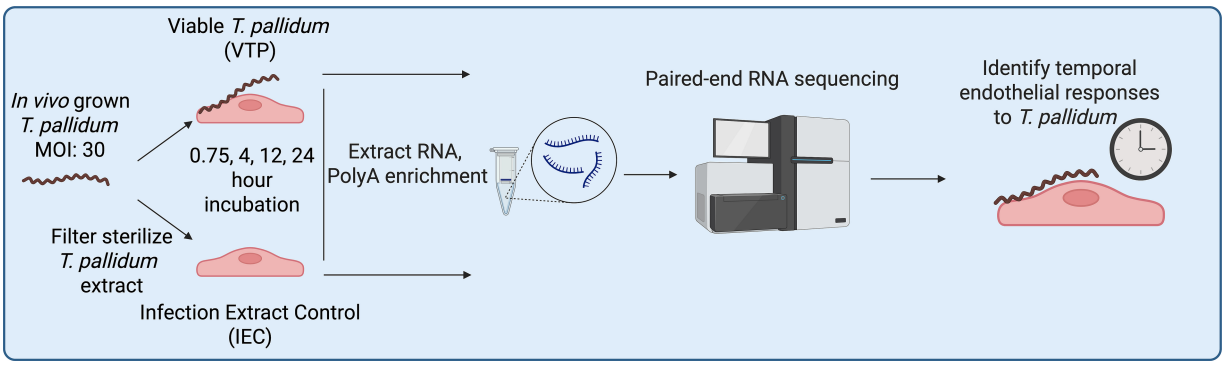

FIGURE 1
RNA sequencing sample generation workflow.

Health, and the United States Department of Agriculture in facilities accredited by the American Association for the Accreditation of Laboratory Animal Care and the CCAC. Institutional biosafety approval was obtained under biosafety certificate 13,170–010. Nichols strain *T. pallidum* was cultured *in vitro* with Sf1Ep cells as previously described (Edmondson et al., 2018) in a HeraCell Vios 160i incubator (Thermo Fisher Scientific, San Jose, CA), with the modification that treponemes were dissociated from Sf1Ep cells using trypsin-free dissociation media (Edmondson and Norris, 2021) for 30 min at 34 °C in 1.5% O_2, 5% CO_2, 93.5% N_2 to maintain the integrity of the *T. pallidum* outer membrane (Edmondson et al., 2018). Bacteria were quantitated by darkfield microscopy (Nikon Eclipse E600; Nikon Canada, Mississauga, Ontario) using a Petroff-Hauser counting chamber (Hauser Scientific, Horsham, PA).

Viable *T. pallidum* (VTP) and infection extract control (IEC) sample preparations

In vivo grown *T. pallidum* was used for RNA-seq assays, and *in vitro* grown *T. pallidum* was used for western blot and microscopy assays. *In vivo Treponema pallidum* subsp. *pallidum* was extracted in *Treponema pallidum* culture medium 2 (TpCM2) formulated as previously described (Edmondson et al., 2018), or harvested *in vitro* as described above. Viable *T. pallidum* (VTP) and infection extract control (IEC) samples were prepared as described previously (Waugh et al., 2023). Briefly, extracts were centrifuged to remove rabbit testicular material and diluted equivalent to working *T. pallidum* concentrations. The viable treponeme suspension contained in one supernatant [designated viable *T. pallidum* (VTP)] was kept for endothelial co-incubation analyses as described below. The second supernatant was further processed to remove *T. pallidum* through sterile filtration with a 0.22 µm cellulose acetate syringe filter (Avantor, Allentown, PA) to create an optimal comparator control (designated infection extract control [IEC]) that contained a level of rabbit testicular or Sf1Ep protein background mirroring the VTP sample. Removal of *T. pallidum* from the IEC sample was confirmed by darkfield microscopy (Nikon Eclipse E600; Nikon Canada, Mississauga, Ontario) and *T. pallidum*-specific qPCR, which measured a 49x reduction in *T. pallidum* FlaA copies in the VTP versus IEC samples.

Endothelial culture and endothelial-*T. pallidum* exposure conditions

Human cerebral brain microvascular endothelial cells (hCMEC/d3; Cedarlane, Burlington, ON), an immortalized cell line, also referred to as HBMECs, were grown to 90% confluence in 6-well tissue culture plates (Corning, Corning, NY), at 5% CO_2 in EndoGRO-MV complete culture medium (Millipore, Etobicoke, ON) at 37 °C in 5% CO_2 in a Forma Series II incubator (Thermo Fisher Scientific). Each well was observed via an Olympus CKX41 inverted microscope for successful HBMEC growth prior to incubation at 34 °C in a microaerophilic environment of 1.5% O_2, 5% CO_2, 93.5% N_2 with 3 mL of either *in vivo* grown VTP (3.0×10^7 *T. pallidum* per well), or equivalent dilutions of IEC for 45 min, 4, 12, and 24 h. At each timepoint, there were 5 replicates of VTP- and 5 replicates of IEC-exposed HBMEC sample wells. Therefore, individual wells are defined as separate biological replicates. At each timepoint prior to cell lysis and RNA harvesting, *T. pallidum* organisms were visually observed for motility via darkfield microscopy (Nikon Eclipse E600).

Following treponemal viability assessment, HBMEC cells were quickly washed 3x in cold PBS and incubated in a 1:1 ratio of Qiagen RNAprotect Cell and Qiagen RNAprotect Bacteria (Qiagen, Toronto, ON) for 10 min on ice to inactivate RNases and stabilize RNA. Cells were pelleted at 10,000×*g* for 10 min, resuspended in 1 mL of fresh RNAprotect cell, stored at −80 °C for downstream processing. RNA was extracted using the Qiagen RNeasy kit according to manufacturer instructions, with the addition of an on-column DNA digestion using RNase-Free DNase (Qiagen). To prevent RNA degradation, 1 µL of SUPERase-In RNase inhibitor was added to the eluted RNA (Qiagen).

RNA integrity analysis, cDNA generation, RNA sequencing, and data analysis parameters

Prior to cDNA library generation, RNA integrity of each sample was assessed by an Agilent Bioanalyzer 2,100 on an RNA 6000 nanochip (Agilent; Santa Clara, CA), where all RNA samples exceeded an RNA integrity value of 8. Samples then underwent PolyA enrichment using NEBNext Poly(A) mRNA Magnetic Isolation Module (catalog no.: E7409L, NEB; Ipswich, MA). Strand-specific cDNA library preparation was generated at the same time for each sample from polyA-purified RNA with a Roche KAPA HyperPrep Kit (Roche; Basel, Switzerland), followed by the addition of unique 8 bp NGS RNA adaptors to identify samples during multiplexed sequencing (NEXTFLEX; PerkinElmer, Woodbridge, ON), generating cDNA with unique tags for each individual sample. cDNA libraries were amplified using adapter primers, followed by purification beads according to manufacturer instructions (NEXTFLEX; PerkinElmer). Amplified DNA quality was assessed on a bioanalyzer using a high sensitivity DNA chip (Agilent) to assess the fragmentation profile and confirm the absence of adaptor-specific primer dimers. cDNA library concentrations were assessed using Qubit QuantIT HS DNA kit (Thermo Fisher Scientific). Each sample was normalized to 4 nM and pooled. Pooled samples underwent paired-end sequencing with a read length of 150 bp on an Illumina HiSeqX (Illumina; San Diego, CA, USA) at the Michael Smith Genome Sciences Center (BC, Canada). Sequence quality was assessed using FastQC v0.12.1 and MultiQC v1.13 (Ewels et al., 2016). The FASTQ sequence reads were aligned to the hg19 human genome (Ensembl GRCh38.98) using STAR v2.7.10b (Dobin et al., 2013) and mapped to Ensembl GRCh38 transcripts. Read-counts were generated using htseq-count (HTSeq 2.0.2) (Anders et al., 2015). All data processing and subsequent differential gene expression analyses were performed using R version 4.4.0 and DESeq2 (Love et al., 2014) version 1.14.1. Genes with very low counts (with less than 10 counts) were pre-filtered and removed *in silico*. Differentially expressed genes were identified using paired analysis with the Wald statistics test and filtering for any genes that showed ±1.5-fold-change (FC) with adjusted *p*-values ≤ 0.05 (cut-off at 5% false discovery rate) as the threshold. Pathway overrepresentation analyses were completed using the Reactome database (Gillespie et al., 2022) annotations and Sigora (v3.1.1) (Foroushani et al., 2013)

pathway overrepresentation, and the molecular signature database (Liberzon et al., 2015) (MSigDB) hallmark gene set analysis was performed using PathlinkR (Blimkie et al., 2024). The packages maSigPro (v1.74.0) (Nueda et al., 2014), and the ClusterProfiler R package (v4.10.0) (Yu et al., 2012) were used for figure generation. For Sigora and MSigDB analyses, q-values were set at 0.05 using the Benjamini-Hochberg (BH) correction, and pathways or cellular compartments with a corrected p-value ≤ 0.05 were considered significant. Transcription factor analysis was completed using the Chea3 integrated mean ranking algorithm (Keenan et al., 2019) for each timepoint.

Western blotting

Confluent HBMECs in 6-well plates were exposed to *in vitro* grown VTP (3×10^7 *T. pallidum* per well), equally diluted IEC, or basal TpCM2 media for 12 and 24 h with 3 biological replicates (defined as individual wells) per treatment condition. Cells were lysed for 30 min on ice with gentle agitation in RIPA lysis buffer containing EDTA-free Protease inhibitor cocktail set 3 (Calbiochem, San Diego, CA) and PhosSTOP phosphatase inhibitor (Roche, Mississauga, ON) according to the manufacturer's instructions. For western blotting, protein concentrations were determined using a BCA assay (Thermo Fisher Scientific). Whole cell lysate (13.5 µg per lane) was subjected to SDS-PAGE using Bolt 12% acrylamide gels (Thermo Fisher Scientific) and transferred to PVDF membrane (Millipore) via wet-transfer at 400 mA for 2 h, and blocked with Intercept TBS blocking buffer (Licor, Lincoln, NE). Rabbit Anti-Snail (CD15D3; 1:1000; Cell Signalling Technology, Danvers, MA; 3879S) and mouse anti-GAPDH (1:1000; Abcam, Ab8245) were used as primary antibodies, while the secondary antibodies used were goat anti-rabbit IgG IRDye 800CW (1:20,000) and goat anti-mouse IgG IR Dye 680RD (1:20,000; Licor). Detection and analysis were completed on a Licor Odyssey CLx using Licor Image Studio version 5.2. Data was tested for normality using a Shapiro-Wilks tests which determined that the data was consistent with normal distribution, and statistical analysis to determine increases in Snail abundance was completed using One-way ANOVA followed by Tukey's multiple comparisons testing.

Treponema pallidum-endothelial co-incubation and F-actin staining

hCMEC/d3 endothelial cells were seeded into black wall µClear cell culture-treated bottom 96-well culture plates (Greiner Bio-one, Monroe, NC; 655090) at 24,000 cells/well and grown overnight as described above to achieve 90–95% confluence. *In vitro* cultivated *T. pallidum* was cultured as described above, then VTP and IEC samples were generated as described above and diluted to 4.34×10^6 cells/mL in TpCM2 media, or equivalent dilution for IEC. For *T. pallidum*-HBMEC co-incubation, HBMEC media was removed, then replaced with 100 µL of VTP, IEC, basal TpCM2 media, or 10 nM bovine thrombin in TpCM2 (Thermo Fisher Scientific; RP-43104) in triplicate per condition, resulting in a multiplicity of infection (MOI) of 30 for VTP samples or equivalent dilution for IEC. Incubations were completed for 15 min, 30 min, or 2 h after the addition of *T. pallidum*, and all incubations were performed at 34 °C in a microaerophilic environment of 1.5% O_2, 5% CO_2, 93.5% N_2 in a HERAcell vios 160i incubator (Thermo Fisher Scientific). At the specified timepoints, *T. pallidum*-containing supernatants were removed and assessed for motility via darkfield microscopy, where *T. pallidum* motility remained greater than 80% for all timepoints. Simultaneously, HBMECs were washed 2x in pre-warmed PBS, fixed in 3.7% formaldehyde in PBS without methanol for 10 min at RT, and washed 3x in pre-warmed PBS. Cells were permeabilized in 0.1% Triton 100-X for 5 min, washed 3x in pre-warmed PBS, and blocked in PBS 1% bovine serum albumin (Thermo Fisher Scientific) for 1 h at 37 °C. Alexa fluor 488 Phalloidin (Thermo Fisher Scientific; A12379) stocks were resuspended in DMSO, then diluted to a 1x working solution in PBS with 3 µM DAPI counterstain (4′,6-diamidino-2-phenylindole; Sigma Aldrich). Fifty microliters of staining solution was added to each well, the plates were incubated at RT for 20 min, washed 3x in warm PBS, and 100 µL PBS was added to each well for imaging.

Cell imaging and image processing

All cell imaging was performed on a Cytation 5 Imaging Reader (Agilent) with a 20x objective. For statistical analyses wells were imaged in the centre of each well in a 3 × 3 field of view square. Images underwent image pre-processing and image deconvolution, after which they were stitched into a single image using linear blending in Gen5 (Agilent; v3.12). All imaging was automated and completed at the same time, and with identical imaging conditions. HBMECs were identified (defined as "objects") and were counted using the DAPI filter as a primary mask (7–35 µm). To determine HBMEC cellular boundaries, a secondary mask was set by expanding the primary DAPI mask (110 µm) in the GFP (FITC; F-actin) channel using the threshold in mask method (FITC; F-actin); touching objects were split, objects contacting the border of the image were excluded, and gaps in masks were filled. Using the secondary mask, F-actin fluorescence intensity was determined within the boundaries of each object, the fluorescence intensity was calculated for each defined object, and the average object fluorescence intensity was calculated for each well. Significant increases in fluorescence intensity were determined by comparing mean object fluorescence intensity from 3 biological replicates (defined as individual wells) per sample condition. Data was tested for normality using a Shapiro-Wilks tests which determined that the data was consistent with normal distribution, and significance was determined using One-way ANOVA followed by Dunnett's multiple comparison, using HBMECs exposed to basal media as the baseline for statistical comparison.

Results

Endothelial transcription was significantly altered during *T. pallidum* exposure

To identify HBMEC genes that were differentially expressed (DE) during *T. pallidum* exposure, RNA-Seq was conducted on five independent wells per treatment condition comparing a viable *T. pallidum* (VTP) exposure to an infection extract control (IEC) exposure at each timepoint. Briefly, these conditions corresponded to

exposure to a VTP sample containing viable *T. pallidum* (viability confirmed by visual assessment of motile treponemes via darkfield microscopy), alongside exposure to an IEC sample where *T. pallidum* was removed using a centrifugation and filtration technique that retains background culture contaminants co-purified during *T. pallidum* harvest (Waugh et al., 2023). Exposing HBMECs to *T. pallidum* significantly altered gene expression in the brain endothelial cells, where the number of DE genes with adjusted *p*-value of < 0.05 and a fold-change (FC) cutoff of ±1.5 were 11 at 45-min, 225 at 4-h, 490 at 12-h, and 1,753 at 24-h (Figures 2A–D; Supplementary Table 1). Considerable overlap in DE genes was observed between timepoints, where 311 genes were differentially expressed at both 12 and 24 h, 52 genes were differentially expressed from 4–24 h, and 4 genes were differentially expressed at all timepoints (Figure 2E).

Treponema pallidum exposure altered expression of transcription factors associated with cellular differentiation

Next, we completed Transcription factor (TF) enrichment and co-regulatory analyses (Keenan et al., 2019) on each of the study timepoints to identify TFs that may be responsible for the observed changes in gene expression in HBMECs during *T. pallidum* exposure. Using an integrated mean ranking algorithm (Keenan et al., 2019), local TF co-regulatory networks were generated for the top 10 TFs predicted to be most influential in regulating the expression of the DE genes at each timepoint (Table 1; Figures 3A–D; Supplementary Tables 2–5). These analyses identified highly connected co-regulatory TF networks at each timepoint, all of which featured AP-1 (Activating Protein-1) subunits such as Fos, FosB, and Jun (Table 1; Figures 3A–D). Notably, the transcripts for *FOS*, *FOSB*, *JUN*, *JUNB*, and *JUND* were upregulated at one or more timepoints in this study (Table 1; Supplementary Table 1). NR4A1 (Nuclear Receptor subfamily 4 group A member 1) and NR4A3 were also enriched at the 12- and 24-h timepoints, and transcripts encoding these TFs were significantly upregulated at all timepoints in the study (Table 1). Transcription factors involved in the cellular differentiation processes of EndMT and Epithelial to mesenchymal transition (EMT) were also enriched at all timepoints, including HEY1 (Hes-related family bHLH transcription factor with YRPW motif 1), HEY2, BHLHE40 (Basic Helix–Loop–Helix Family Member e40), EGR1 (Early Growth Response 1), and EGR2 (Table 1). Snail, the primary TF driving EndMT (Kokudo et al., 2008; Derada Troletti et al., 2019; Ma et al., 2021) ranked among the top 10 most enriched TFs for all timepoints (Supplementary Tables 2–5). Significantly increased *SNAI1* transcripts were observed in VTP-exposed HBMECs from 12- to 24-h (3.08, 3.11 FC, respectively), contrasting with minimal alteration of *SNAI1* transcripts in IEC-exposed HBMECs over the same period (Table 1; Figure 4A). Western blot validation confirmed *T. pallidum* exposure induced Snail protein upregulation, with significantly higher protein abundance at 24 h and increased protein abundance at 12 h (VTP-versus IEC-exposed cells; Figures 4B,C). Collectively, these findings identify the early and sustained alteration of EndMT-associated TFs and their influence on HBMEC transcriptional responses to *T. pallidum* exposure.

Treponema pallidum exposure altered pathways within the categories of gene expression, extracellular matrix organization, immune system, programmed cell death, and signal transduction

We next performed Sigora pathway overrepresentation analysis (Foroushani et al., 2013) on up- and down-regulated genes at each timepoint to investigate pathways that are significantly overrepresented in *T. pallidum*-exposed HBMECs. Sigora uses Reactome database annotations (Gillespie et al., 2022) and contextualizes pathway overrepresentation by weighting DE gene pairs that occur uniquely in a single pathway. The number of overrepresented pathways increased with time, with 1, 15, 19, and 46 significantly overrepresented pathways at 45-min, 4-, 12-, and 24-h, respectively. These investigations identified overrepresented cellular pathways within the categories of gene expression, extracellular matrix (ECM) organization, immune system, programmed cell death, disease, and signal transduction, and key pathways from these categories are highlighted below (Figures 5A–D; Supplementary Tables 6–9).

Within the category of gene expression, we observed overrepresentation of pathways related to p53-mediated cell death and p53-mediated transcriptional regulation at the 4- to 24-h timepoints (Figures 5B–D; Supplementary Tables 7–9). At the 12-h timepoint, pathways related to EndMT were upregulated, such as "SMAD2/SMAD3: SMAD4 transcriptional regulation" and "regulation of PTEN gene expression" (Figure 5B; Supplementary Table 7). We also observed dysregulation of pathways involved in ECM organization, with "integrin signaling" first downregulated at 4-h, followed by upregulation of additional ECM pathways ("non-integrin membrane-ECM interactions," "molecules associated with elastic fibres," and "signaling by receptor tyrosine kinases") at 24-h (Figures 4D, 5B; Supplementary Tables 7, 9). Within the category of immunity, we observed downregulation of pathways in "chemokine receptors bind chemokines" and TNF and IFN signaling (4- and 12-h), suggesting inflammatory pathway downregulation (Figures 5B,C). While "chemokine receptor signaling" remained downregulated at 24-h, pathways involving TNF and IFN signaling were upregulated, indicating differential temporal regulation of these immune pathways in HBMECs exposed to *T. pallidum* (Figure 5D).

Within the category of signal transduction, we observed the pathway "negative regulation of MAPK (Mitogen-Activated Protein Kinase)" to be upregulated at 4- and 12-h, and "RAF/MAP kinase cascade" to be downregulated at 12-h, indicating the involvement of MAPK signaling in the endothelial response to *T. pallidum*. At the 24-h timepoint, overrepresented pathways within the category of signal transduction included "downregulation of TGFβ receptor signaling," and upregulation of "NOTCH4 intracellular domain regulates transcription," "signaling by receptor tyrosine kinases," and "diseases of signal transduction," indicating the potential for *T. pallidum* to modulate a range of endothelial signaling pathways during exposure (Figure 5D). Further, pathways related to Rho GTPase activity were downregulated at 4- and 24-h, however the downregulated genes in these pathways are primarily GTPase-activating proteins (GAPs) which negatively regulate Rho GTPases (Supplementary Tables 7, 9). Relatedly, the Rho GTPase-mediated pathway "Sema4D induced cell migration and growth cone collapse"

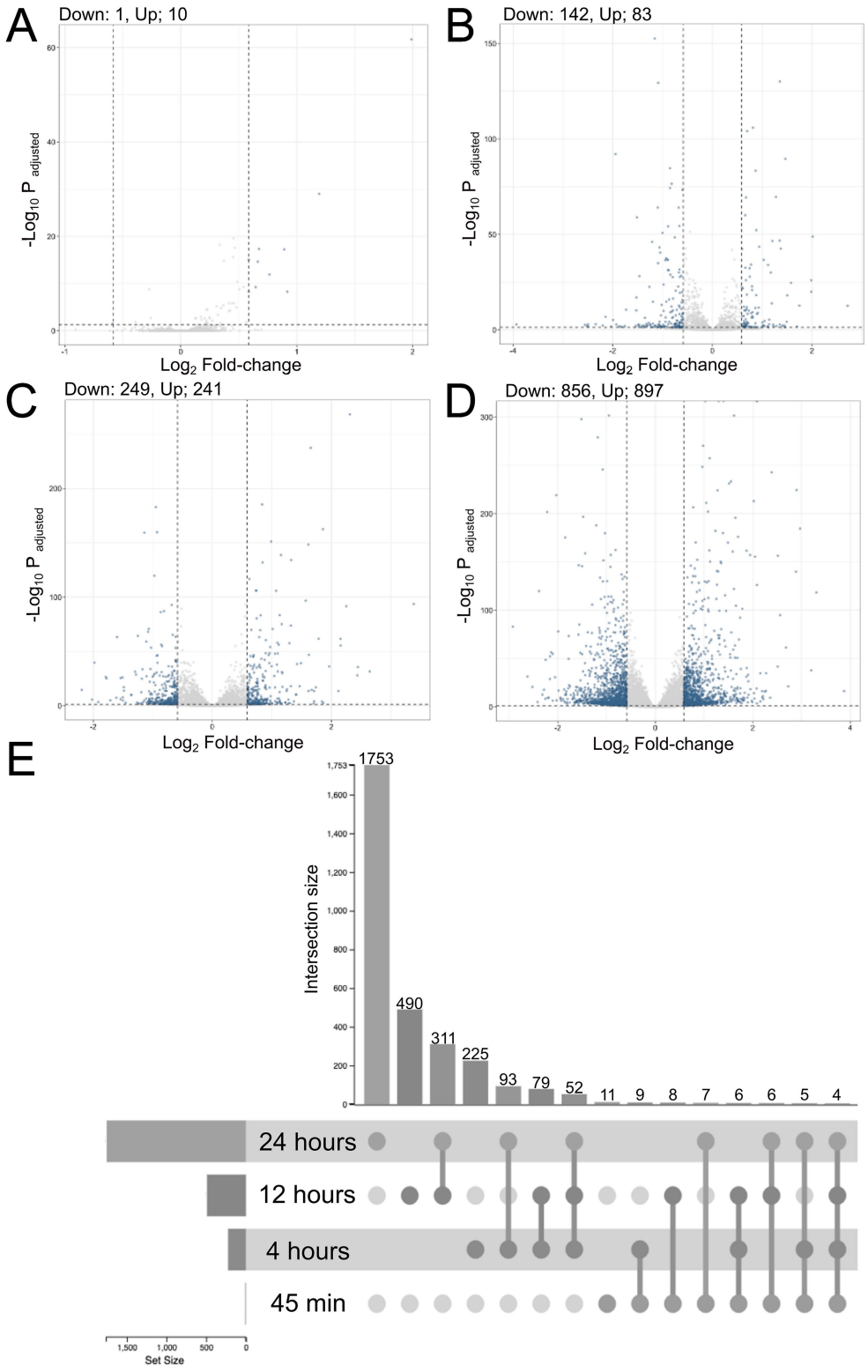

FIGURE 2
The number of DE genes in VTP versus EC-exposed cells increased with longer *T. pallidum* exposure times, and DE genes demonstrated significant overlap between timepoints. Volcano plots showing DE genes at **(A)** 45-min, **(B)** 4-h, **(C)** 12-h, and **(D)** 24-h exposures. Dotted lines denote a fold-change cutoff of ±1.5, and an adjusted *p*-value cutoff of 0.05. Significant DE genes are blue, non-significant genes are light grey. The number of up- and downregulated genes per timepoint is shown above the plot. **(E)** Upset plot showing the intersection of DE genes between timepoints.

TABLE 1 Fold change of genes encoding transcription factors ranked by transcription factor enrichment analysis to be among the top 10 most influential transcription factors at one or more timepoints.

Gene	45 min FC	5 h FC	12 h FC	24 h FC
ARID5A				2.55
ATF3			3.45	7.83
BHLHE40			1.75	1.54
CENPA			−1.56	−1.61
CREB5				3.02
CSRNP1			2.02	3.12
EGR1	−1.50		10.44	2.13
FOS			6.25	1.75
FOSB			2.76	2.28
HEY2				3.24
JUN			1.58	
NR4A1	1.50	2.30	4.76	3.21
NR4A3	3.97	1.74	2.68	2.93
RELB				1.79
SNAI1			3.08	3.11
TWIST1			−1.84	−2.05

and "Rho GTPase activates NADPH oxidases" were upregulated at 12- and 24-h, respectively (Figures 5C,D).

To identify temporal connections between overrepresented pathways, we next performed pathway network analysis at each timepoint, to identify pathway clusters and connections based on overlapping DE genes (Figures 6A–D). Through this analysis we determined that the relationships between overrepresented pathways became more connected with longer *T. pallidum* exposures (Figures 6A–D). At earlier timepoints, pathways formed distinct clusters which were separated into categories such as immune responses and signal transduction (Figures 6A–C). The 24-h network showed the most connections within and between clusters of pathways, including connections between clusters belonging to different categories (Figure 6D), suggesting a converging transcriptional trajectory in *T. pallidum*-exposed HBMECs.

Treponema pallidum exposure resulted in overrepresentation of hallmark gene sets in the categories of development, immune responses, cellular signaling, and cellular stress

To identify higher-order overrepresented transcriptional profiles in HBMECs exposed to *T. pallidum*, we performed hallmark molecular signature enrichment analysis using the MSigDB database (Liberzon et al., 2015) on each study timepoint. Hallmark gene sets are curated and contextual, whereby gene function is considered for direction of regulation. Due to this context, and the higher-order approach to pathway analysis, hallmark gene sets can be both up- and downregulated at single timepoints. Through these analyses, we identified hallmark gene set overrepresentation within the categories of development, immune, signaling, and stress (Figures 7A–D), supporting the results of the Sigora pathway overrepresentation analysis. Consistent with the pathway analysis, hallmark gene set enrichment also identified inflammatory gene sets to be downregulated. Additionally, the gene set "TNF-α signaling through NF-κB" was simultaneously up- and downregulated at all timepoints, resulting from concurrent differential regulation of genes belonging to these pathways (Figures 7A–D). Further, the "apoptosis" gene set was overrepresented at all timepoints, although the direction of regulation varied (Figures 7B–D). We also observed overrepresented gene sets within the signaling category, including downregulation of "KRAS signaling UP" from 4- to 24-h, and upregulation of both "Wnt β-catenin signaling" and "NOTCH signaling" at 24-h (Figures 7B–D).

In support of the overrepresented TGFβ and SMAD signaling pathways identified by Sigora pathway analysis, in the hallmark gene set "TGFβ signaling" was also upregulated from 45-min to 12-h (Figures 7A–C). Notably, the "epithelial to mesenchymal transition (EMT)" gene set was both up- and downregulated from 4- to 24-h, with upregulation being most significant at these timepoints (Figures 7A–D). This bi-directional regulation reflects the dynamic regulation of this cellular process. Currently, there is no hallmark gene set for EndMT; however, EMT and EndMT have shared regulatory pathways (Saito, 2013), and thus this analysis provides insight into the regulatory factors common to both pathways. Additional EMT- and EndMT-related hallmark gene sets were overrepresented at the 24-h timepoint, such as "myogenesis" and "angiogenesis" (Figure 7D; Supplementary Table 13). These data reinforce that EndMT-inducing pathways and gene sets, such as TGFβ, SMAD, and NOTCH signaling, and *SNAI1* transcription/Snail protein expression were induced in HBMECs exposed to *T. pallidum*.

We observed that many genes involved in EndMT-related processes were DE, including upregulation of the SMAD negative regulator *PMEPA1* (Prostate transmembrane Protein Androgen Induced 1) and inhibitory *SMAD7*, as well as downregulation of activating *SMAD3*. Genes associated with *SNAI1* overexpression (Pinto et al., 2018) were also DE, such as upregulation of the EndMT-promoting ECM component *FBLN5* (Fibulin-5), and downregulation of adhesion molecules (Li et al., 2021) *ICAM-1* (Intercellular Adhesion Molecule 1), *VCAM-1* (Vascular Cell Adhesion Protein 1), as well as genes encoding junctional proteins, including *CLDN1* (Claudin-1), *OCLN* (Occludin), and *ZO-2* [Zona Occludens-2 (also known as *TJP2*)] (Table 2; Supplementary Table 1). *vWF* (von Willebrand Factor), a secreted factor important for endothelial inflammation, angiogenesis, endothelial dysfunction, and adhesion of platelets and leukocytes to endothelial cells (Randi and Laffan, 2017), was upregulated at the 12- and 24-h timepoints (Table 2; Supplementary Table 1). Mesenchymal marker transcripts (Piera-Velazquez and Jimenez, 2019) were increased, including upregulation of *SM22-α* [Smooth Muscle Protein 22 Alpha (also called *TAGLN*)], *α-SMA* [Smooth Muscle Actin Alpha 2 (also called *ACTA2*)], *Integrin-β3*, *ACTC1* (Actin Alpha Cardiac Muscle 1), *COL3A1* (Collagen type III A1), *COL4A1*, *COL4A2*, *POSTN* (Periostin), and *FN1* (Fibronectin) (Table 2; Supplementary Table 1). These data demonstrate that HBMECs exposed to *T. pallidum* undergo significant transcriptional alterations consistent with the process of EndMT, and identified the involvement of Snail in the host endothelial response to *T. pallidum*.

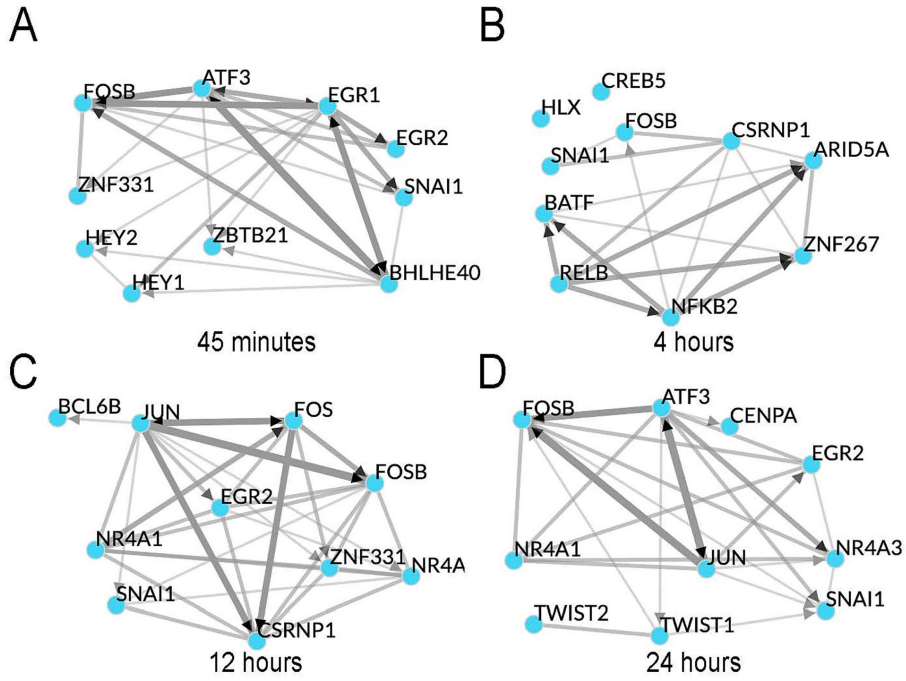

FIGURE 3
Transcription factor enrichment revealed the top 10 most enriched TFs at each timepoint form highly connected co-regulatory networks. Shown are Chea3 transcription factor enrichment integrated mean analyses for the timepoints **(A)** 45-min, **(B)** 4-h, **(C)** 12-h, **(D)** 24-h. Edge (line) width represents the strength of interaction from chromatin immunoprecipitation sequencing (ChIPseq), co-expression, and co-occurrence data. Black arrowheads indicate the direction of co-regulation where ChIP-seq supports the direction of regulation, and undirected (no arrows) where only co-occurrence or co-expression data is available.

Growth factor pathways and genes involved in EndMT are altered in HBMECs exposed to *T. pallidum*

We found that HBMECs exposed to *T. pallidum* demonstrated transcriptional alteration indicative of TGFβ and SMAD signaling, as well as pathways that modify TGFβ signaling such as NOTCH1, Wnt/β-catenin, and receptor tyrosine kinase (RTK) signaling, all of which contribute to EndMT (Figures 5, 7; Supplementary Tables 6–13). Importantly, TGFβ signaling is controlled through feedback loops, particularly negative feedback, where genes induced by TGFβ signal activation both attenuate the activity of TGFβ signaling proteins and repress transcription of genes involved in TGFβ signaling (Yan et al., 2018). The findings in the current study are consistent with the activation and downstream regulation of TGFβ signaling. Specifically, Sigora pathway analysis identified upregulation of the pathway "SMAD2/SMAD3: SMAD4 heterotrimer regulates transcription" at 12-h, which is the primary transcriptional response induced by TGFβ signal activation (Yan et al., 2018) (Figure 6C). Negative feedback was also evident through upregulation of the pathway "downregulation of TGFβ receptor signaling" at 24-h, where the DE genes in this pathway are upregulated as a negative feedback response to TGFβ signal activation (Figure 7D). Further, hallmark gene set analysis, which accounts for the context and function of DE genes, identified upregulation of TGFβ signaling from 45-min to 12-h (Figures 7A–C). These data indicate the activation and regulation of TGFβ signaling pathways in the endothelial response to *T. pallidum*.

To further investigate these findings, we assessed the transcript level changes of specific growth factor genes involved in EndMT-activating and regulatory pathways. Specific DE genes within TGFβ signaling include the downregulation of *TGFBR* (TGFβ Receptor)-*2* and *−3* at 12- and 24-h, and *SMAD3*, a prominent activating TF downstream of TGFβ signaling, at the 4- and 12-h timepoints (Table 2; Supplementary Table 1). Expression of TGFBRs is negatively regulated by genes induced by TGFβ signaling, such as the inhibitory *SMAD7*, which is induced by the SMAD2/SMAD3: SMAD4 dimer as a negative feedback mechanism (Yan and Chen, 2011; Yan et al., 2018) and was upregulated in this study (Table 2; Supplementary Table 1). Upregulation of additional TGFβ-induced negative regulators (Yan et al., 2018) was observed, including *BAMBI* (BMP and Activin Membrane Bound Inhibitor) at 24-h, and *PMEPA1* at 12- and 24-h (Table 2; Supplementary Table 1). Additional upregulated TGFβ-induced genes (Watanabe et al., 2010; Ma et al., 2021) include *ID* (Inhibitor of DNA binding)-*1*, *−2*, and *−3*, and fibrosis regulator (Nakerakanti et al., 2011) *CCN2* (Cellular Communication Network Factor 2) (Table 2; Supplementary Table 1). Upregulated genes that enhance TGFβ and EndMT include *EDN1* (Endothelin-1) at 4- to 12-h, and *POSTN* (Periostin) that is involved in TGFβ-induced EndMT/EMT through integrin-β3 signaling (Yue et al., 2021), which was upregulated at 24-h (Table 2). These data demonstrate the activation and regulation of TGFβ signaling in HBMECs exposed to *T. pallidum*.

TGFβ can also signal independently of SMADs, including through pathways involving MAPK cascades, GTPases, and Wnt/β-catenin (Piera-Velazquez and Jimenez, 2019). In the current study,

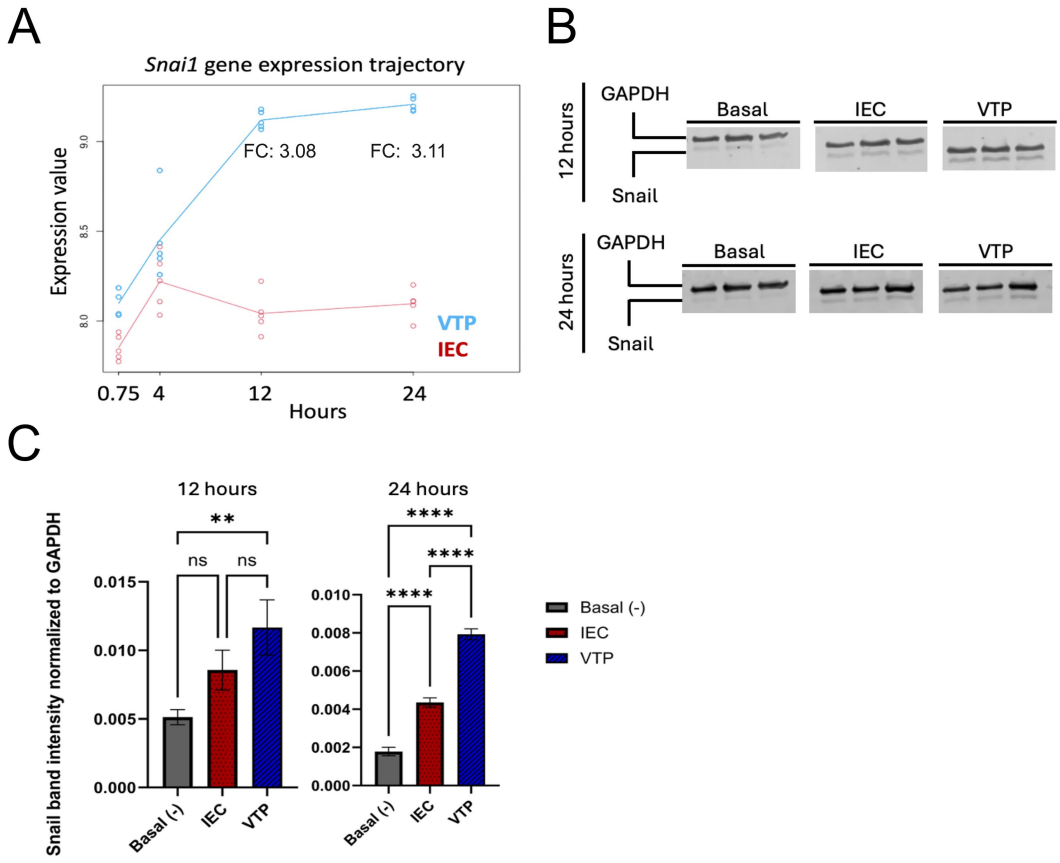

FIGURE 4
SNAI1 gene and Snail protein expression was increased in HBMECs exposed to *T. pallidum*. **(A)** *SNAI1* (Snail) longitudinal expression plot showing log-transformed expression values at each timepoint for viable *T. pallidum* exposed cells (VTP; Blue) versus infection extract control (IEC; Red). Each data point represents an individual biological replicate. Analysis and figure generation completed using maSigPro (v1.74.0). **(B)** Temporal analysis of Snail protein expression in endothelial cells exposed to VTP, IEC, and Basal Media conditions. Each condition comprises three biological replicates, defined as individual tissue culture wells exposed to the treatment conditions. GAPDH was used as a loading control and for normalization. The 12- and 24-h timepoints were run on separate gels. Empty lanes separating different sample conditions (Basal, IEC, and VTP) were removed. **(C)** Quantification of Snail protein abundance normalized to GAPDH as a loading control. Quantitation was completed on a Licor Odyssey CLx using Licor Image Studio version 5.2. Significant differences in Snail abundance determined by one-way ANOVA followed by Tukey's multiple comparisons test, where comparisons were considered significant with a p-value ≤ 0.05. indicates a p-value ≤ 0.05, ** indicates a p-value ≤ 0.01, *** indicates a p-value ≤ 0.001, and **** indicates a p-value ≤ 0.0001.

we observed significant overrepresentation of these signaling pathways at one or more timepoints, as determined by both Sigora and hallmark gene set overrepresentation analyses (Figures 5, 7; Supplementary Tables 6–13). Among these pathways, *DUSP2* (Dual Specificity Phosphatase 2) and *DUSP8* were among the most upregulated genes, indicating negative feedback of MAPK signaling (Table 2). Other regulators in the EndMT and non-canonical TGFβ pathways include the upregulation of *NECTIN4* and *IL-11*, the latter of which contributes to fibrosis and EndMT and was upregulated at all timepoints (Table 2) (Schafer et al., 2017; Milara et al., 2022). Correspondingly, *NOX4* (NADPH oxidase 4), which mediates fibrosis and cellular differentiation downstream of IL-11 and TGFβ (Cucoranu et al., 2005), was upregulated from 4- to 12-h (Table 2). Additionally, *NEDD9* (neural precursor cell expressed, developmentally down-regulated 9), a focal adhesion scaffold protein involved in transducing cell adhesion and integrin signaling through RTKs, as well as promoting EMT and cancer metastasis (Jin et al., 2014), was significantly upregulated at 12 and 24 h (Table 2). Other growth factor signaling genes that contribute to EndMT were also upregulated, including *PDGFB* (Platelet-Derived Growth Factor B), *VEGFA* (Vascular Endothelial Growth Factor A), *PGF* (Placental Growth Factor), and *FLT1*, which encodes VEGF Receptor 1 (VEGFR1) (Table 2). In alignment with the differential expression of growth factors and overrepresentation of growth factor signaling pathways and hallmark gene sets, RTK signaling pathways were significantly overrepresented at the 24-h timepoint (Figure 5D). Collectively, these data demonstrate the alteration and regulation of growth-factor signaling genes and pathways in HBMECs during *T. pallidum* contact.

ECM regulatory factors, components, and pathways were dysregulated during *T. pallidum* exposure

In the current study, we found *T. pallidum*-exposed HBMECs exhibited significant transcriptional alterations of ECM constituents and regulatory proteins, accompanied by overrepresentation of ECM organization and signaling pathways at several timepoints

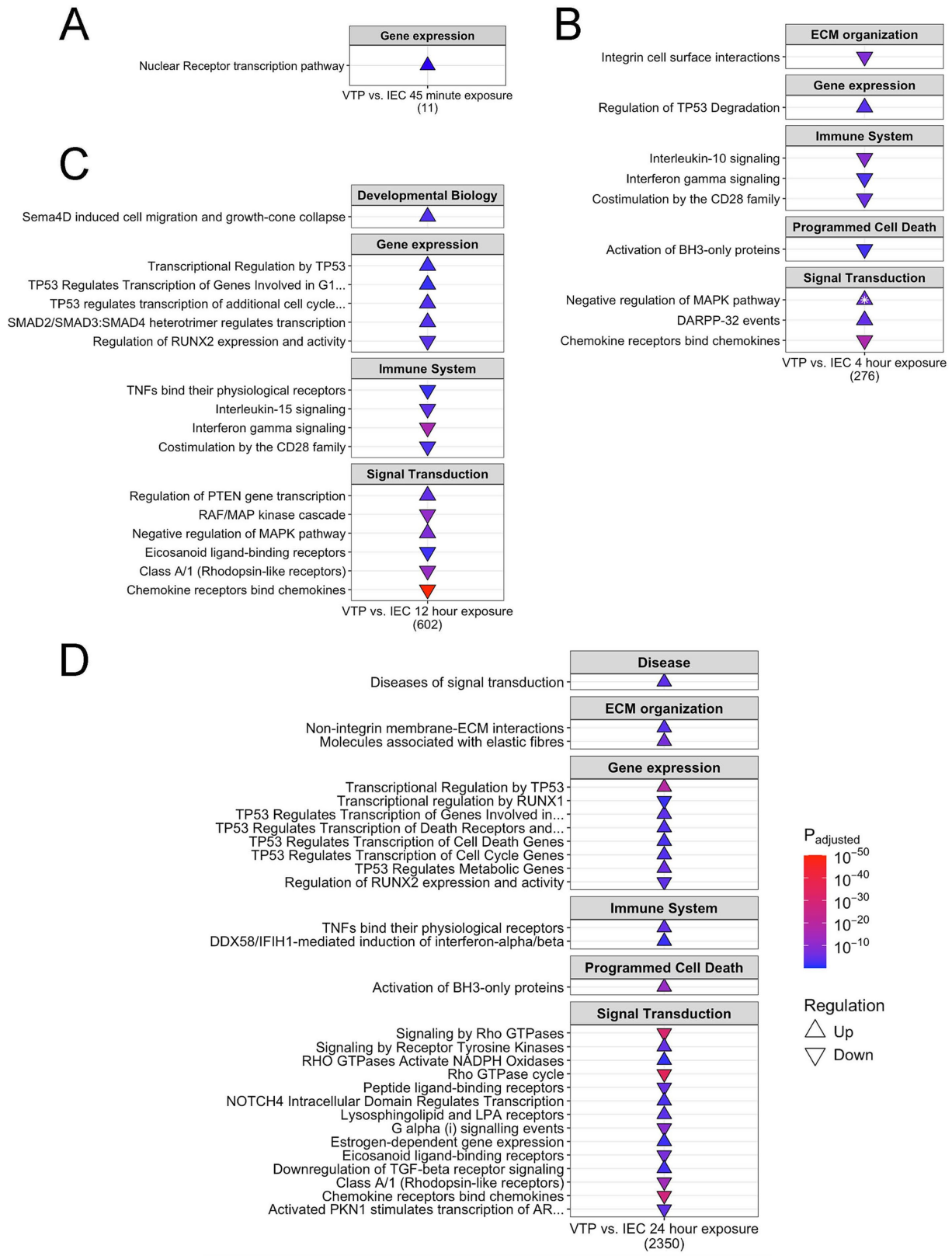

FIGURE 5
Treponema pallidum exposure altered transcription of genes involved in the categories of gene expression, extracellular matrix organization, immune system, programmed cell death, and signal transduction. Shown is a subset of overrepresented pathways in HBMECs exposed to *T. pallidum* that were upregulated (Δ) and downregulated (∇) at the timepoints of **(A)** 45-min, **(B)** 4-h, **(C)** 12-h, **(D)** 24-h. The total number of genes for each timepoint is listed under each table. White stars on the pathway indicate that the pathway was both up- and downregulated, with the direction of arrow indicating

(Continued)

FIGURE 5 (Continued)
the most statistically significant direction of regulation. The subset of overrepresented pathways included align with overarching functional categories described in the results. The full list of overrepresented pathways are listed in Supplementary Tables 6–9.

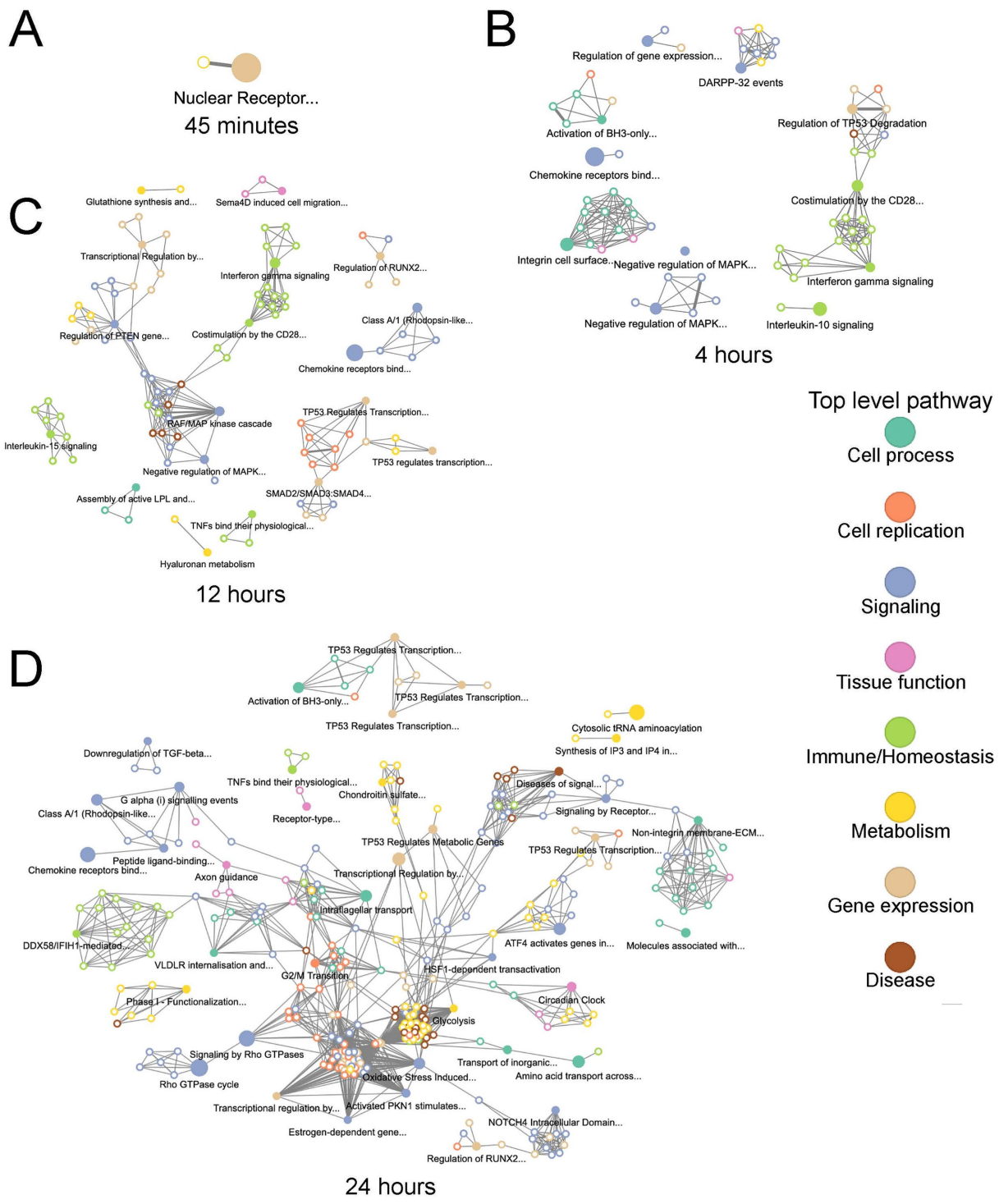

FIGURE 6
Overrepresented pathways in *T. pallidum*-exposed HBMECs became more connected with increased exposure duration. Visualization of networks of overrepresented Reactome pathways at **(A)** 45-min, **(B)** 4-h, **(C)** 12-h, **(D)** 24-h of exposure. Pathway connection is determined using the overlap of the genes assigned to each pathway to determine their similarity to one other. Each node represents a pathway, and the connection/edge connecting nodes was determined using a maximum Jaccard distance of 0.85. Significantly overrepresented pathways are represented by a solid-colored node and have an associated pathway title. The nodes with a colored border and white core are not significantly overrepresented. Nodes are colour-coded according to the legend by top-level pathway. The connections between pathways are represented by the thickness of the edge connecting each node.

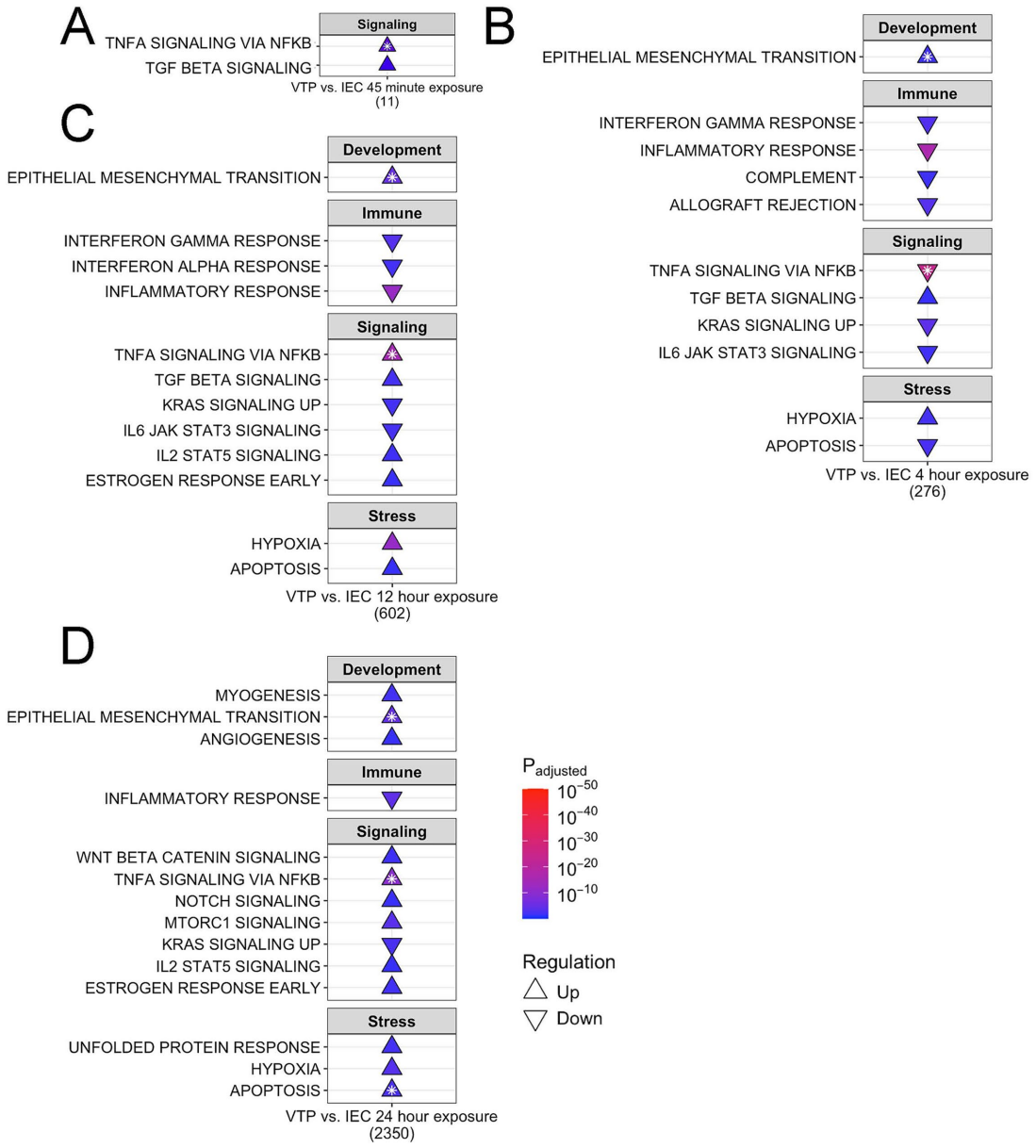

FIGURE 7
Hallmark gene categories of development, immune responses, cellular signaling, and stress were enriched in *T. pallidum*-exposed HBMECs. Shown is a subset of overrepresented hallmark gene sets in HBMECs exposed to *T. pallidum* that were upregulated (Δ) and downregulated (∇) at the timepoints of **(A)** 45-min, **(B)** 4-h, **(C)** 12-h, **(D)** 24-h. The total number of genes for each timepoint is listed under each table. White stars on the pathway indicate that the pathway was both up- and downregulated, with the direction of arrow indicating the direction of regulation with the lowest adjusted *p*-value. The subset of gene sets included align with overarching functional categories described in the results. The full list of overrepresented hallmark genesets are listed in Supplementary Tables 10–13.

(Figures 5B,D; Table 3; Supplementary Tables 7, 9). ECM components that were DE included upregulation of collagen subtypes *3*, *4*, *5*, *7* and *27*, and downregulation of *COL5A3* (Table 3; Supplementary Table 1). The collagen receptor and EMT positive regulator (Walsh et al., 2011), *DDR2* (Discoidin Domain Receptor 2), was also upregulated at 24-h, as were the ECM components *LAMA1* (Laminin subunit alpha 1) and *FN1* (Fibronectin) that have previously been shown to facilitate *T. pallidum* attachment to the endothelium (Cameron, 2003; Cameron et al., 2004; Brinkman et al., 2008) (Table 3; Supplementary Table 1).

We also observed genes encoding ECM modifying proteins to be both up- and downregulated, indicating the dysregulation of endothelial ECM homeostasis during *T. pallidum* exposure. These genes include those belonging to the primary ECM modifying protein families such as MMP (Matrix Metalloproteinase), *ADAM* (A Disintegrin And Metalloproteinases), *ADAMTS* (A Disintegrin And Metalloproteinases with ThromboSpondin Motifs), and *ADAMTSL* (ADAMTS-Like proteinases) (Table 3; Supplementary Table 1). We also observed dysregulation of the plasmin regulation, including upregulation of the endothelial plasminogen activator *PLAT* [Tissue-type plasminogen activator (also known as *tPA*)]. Other related genes included downregulation of the inhibitor of *tPA SERPINB2* [Plasminogen activator inhibitor-2 (also known as PAI-2)], and

10.3389/fmicb.2025.1649738

TABLE 2 Fold change of differentially expressed genes involved in EndMT and growth factor signaling.

Gene symbol	45 min FC	4 h FC	12 h FC	24 h FC
ACTA2				1.98
ACTC1		4.03	4.46	3.76
BAMBI				1.61
CCN2		1.60	1.98	
CLDN1			−1.76	
COL3A1				1.55
COL4A1			1.84	2.09
COL4A2				1.72
DUSP2		6.56	3.64	
DUSP8		−1.73	2.39	9.88
EDN1		1.59	3.06	2.69
FBLN5			1.67	2.09
FLT1			1.61	
FN1				1.62
ICAM1		−1.60		
ID1	2.29	1.60		
ID2	1.89	2.17		1.66
ID3	1.70	1.61		
IL11	1.56	2.42	2.17	2.50
ITGB3			1.52	1.57
NECTIN4				6.42
NEDD9			3.15	2.40
NOX4		1.55	2.25	2.01
OCLN			−1.68	
PDGFB			4.96	2.32
PGF				1.81
PMAIP1				1.88
PMEPA1			2.97	3.15
POSTN				1.66
SMAD3				−1.63
SMAD7			1.94	1.84
SNAI1			3.08	3.11
TAGLN				1.52
TGFBR2			−1.53	−1.67
TGFBR3			−2.11	−2.13
TJP2			−1.58	−1.61
VCAM1		−2.41	−3.94	−2.53
VEGFA			1.67	
VWF			1.52	1.72

TABLE 3 Fold change of differentially expressed genes involved in ECM regulation and cell structure.

Gene symbol	45 min FC	4 h FC	12 h FC	24 h FC
ADAM12				−1.65
ADAM32				1.72
ADAM8				−1.61
ADAMTS10			1.81	
ADAMTS12				−1.54
ADAMTSL5				1.79
CDC42BPG				4.61
COL27A1			1.51	
COL3A1				1.55
COL4A1			1.84	2.09
COL4A2				1.72
COL5A1			1.55	1.85
COL5A3		−1.51		
DDR2				1.77
FN1				1.62
ITGAX		−3.80		
ITGB3			1.52	1.57
ITGB8		−2.29	−2.91	−2.12
LAMA1				1.56
MMP1				−1.51
MMP25		−2.47		
PLAT				1.79
RHOB			2.51	2.03
RHOD				1.56
RHOJ				−1.57
RND1		−1.69	1.87	3.65
SERPINB2		−1.77	−3.46	
SERPINE1			1.79	

upregulation of *SERPINE1* [plasminogen activator inhibitor-1 (also known as PAI-1)] (Table 3; Supplementary Table 1). Notably, *SERPINE1* (PAI-1) expression is induced by TGFβ and Rho/ROCK activation (Samarakoon et al., 2008). Conversely, *SERPINB2* is downregulated in response to TGFβ (Elsafadi et al., 2017). These findings demonstrate that *T. pallidum* exposure induces significant alterations in transcript levels of key ECM components, regulators of ECM deposition and degradation, and activators/inhibitors of the blood plasminogen/plasmin system. Further, these data highlight the importance of the ECM as a signaling and regulatory interface during *T. pallidum*-host interactions.

Treponema pallidum exposure dysregulated cytoskeletal and junction regulatory pathways and altered HBMEC cellular morphology

In our dataset we observed that pathways involving Rho GTPase activity, as well as those that interact with or modulate Rho signaling, such as RTK, ECM, and integrin signaling, were significantly overrepresented at one or more timepoints (Figures 5, 7D;

Supplementary Tables 6–9, 13). Consistent with the overrepresented Rho signaling pathways, Rho GTPases *RHOB*, *RHOD*, *RND1* (Rho family GTPase 1) were upregulated, and *RHOJ* was downregulated (Table 4; Supplementary Table 1). Cdc42 regulators were also DE, including upregulation of the Cdc42-activating protein *CDC42BPG* (Cdc42 binding protein kinase gamma). Several integrins were DE, including upregulation of *ITGB3* at 12- and 24-h, and downregulation of *ITGAX* and *ITGB8* (Table 4; Supplementary Table 1). These findings highlight the dysregulation of Rho GTPases, integrins, and regulators of endothelial junctional dynamics during *T. pallidum* contact.

To further investigate the activation of Rho GTPase signaling in endothelial cells during *T. pallidum* exposure, we performed fluorescent F-actin staining of *T. pallidum*-exposed HBMECs (Figure 8). A subset of HBMECs exposed to *T. pallidum* for 15 and 30 min exhibited a contracted cellular morphology, featuring prominent cortical actin rings and slight membrane blebbing (Figures 8A,B). Mean F-actin fluorescence intensity per cell was significantly higher in HBMECs exposed to *T. pallidum* compared to those exposed to basal media. Similarly, HBMECs treated with a biologically relevant concentration of thrombin showed a trend toward increased fluorescence intensity and displayed a contracted morphology with cortical actin ring formation, resembling the response observed in *T. pallidum*-exposed cells (Figures 8A–D). HBMECs exposed to IEC exhibited moderate contraction and a trend toward increased fluorescence intensity, indicating a cellular response to background components in the *T. pallidum* culture media. These findings highlight the pronounced response of HBMECs to viable *T. pallidum*. These alterations had dissipated at the 2-h timepoint, suggesting a temporal and reversible cellular response to *T. pallidum* engagement (Figure 8C). Additionally, the observed changes in cellular morphology precede alterations in transcription of cell-structure related genes and pathways, which was first observed at the 4-h timepoint. In summary, our transcriptomic analyses identified integrin/non-integrin, ECM, RTK, and Rho GTPase signaling pathways as significantly overrepresented in *T. pallidum*-exposed HBMECs. Microscopy analyses supported these findings by demonstrating HBMEC F-actin contraction during *T. pallidum* exposure, with viable *T. pallidum* inducing endothelial actin cytoskeletal alterations within minutes of contact.

TABLE 4 Fold change of differentially expressed genes involved in immunity and cell death.

Gene symbol	45 min FC	4 h FC	12 h FC	24 h FC
BBC3		−1.75		3.03
BCL2A1			−1.74	−1.91
BCL2L11			1.63	2.18
CASP1				−1.60
CASP8				−1.76
CCL2		−2.03	−2.84	−7.57
CCL20		−2.13	−1.70	−1.86
CSF1		−1.57		
CSF2		−3.85	−1.98	−2.39
CSF3		−2.31	−1.96	−2.53
IFNB1				3.94
IKBKE				−1.60
IRF1		−2.13		
NFKB1				1.71
NFKB2				1.56
PMEPA1			2.97	3.15
TCIM		2.20	4.33	5.12
TNFRSF10C				2.38
TNFRSF1B				−1.93
TNFRSF9		−1.97	−1.78	2.23
TNFSF10			−2.04	−2.10
TNFSF11				−2.14
TNFSF13B			−2.21	
TNFSF15		−1.99		
TNFSF18			−2.05	−2.83
TNFSF4				1.63
TNFSF9				1.79
TP53INP1				1.51
TRAF1		−1.91		3.85
TRAF2				1.59
TRAF4				1.60
TRAF5				−1.58

Treponema pallidum exposure altered interferon, tumor necrosis factor, and inflammatory immune responses

We identified significant dysregulation of immune signaling pathways based on both Sigora and hallmark gene set analyses. Sigora pathway analysis identified the downregulation of chemokine receptor signaling from 4 to 12 h and the downregulation of IFN gamma and TNF signaling pathways at the 4- and 12-h timepoints, followed by upregulation of TNF and IFN alpha/beta signaling at 24 h (Figures 5A–D). Additionally, hallmark gene set analysis identified dysregulation of inflammatory responses from 4- to 24-h (Figures 7B–D). Downregulated genes within these pathways included monocyte recruiting and activating cytokines/chemokines, such as monocyte chemoattractant protein 1 (*MCP-1* or *CCL2*), *CCL20* (Chemokine C-C motif 20), and colony-stimulating factors (*CSF*)*-1*, *CSF2*, and *CSF3* (Figures 5B–D). IFN immune signaling genes included downregulation of *IRF1* (Interferon regulatory factor 1), and upregulation of *IFNB1* (IFN-β) (Table 4; Supplementary Table 1).

TNF hallmark gene sets were differentially regulated at all timepoints in the present study, where the "TNF-α signaling through NF-κB" gene set demonstrated both significant up- and downregulation, reflecting the diverse roles of differentially expressed genes within these pathways (Figures 5, 7; Supplementary Tables 6–13). Indeed, genes encoding TNF receptors (TNFRs) were downregulated from 4- to 12-h and were both up- and downregulated at 24-h (Table 4; Supplementary Table 1). TNFR adaptors such as the TRAF (TNF-receptor-associated factor) family exhibited differential expression, primarily at the 24-h timepoint

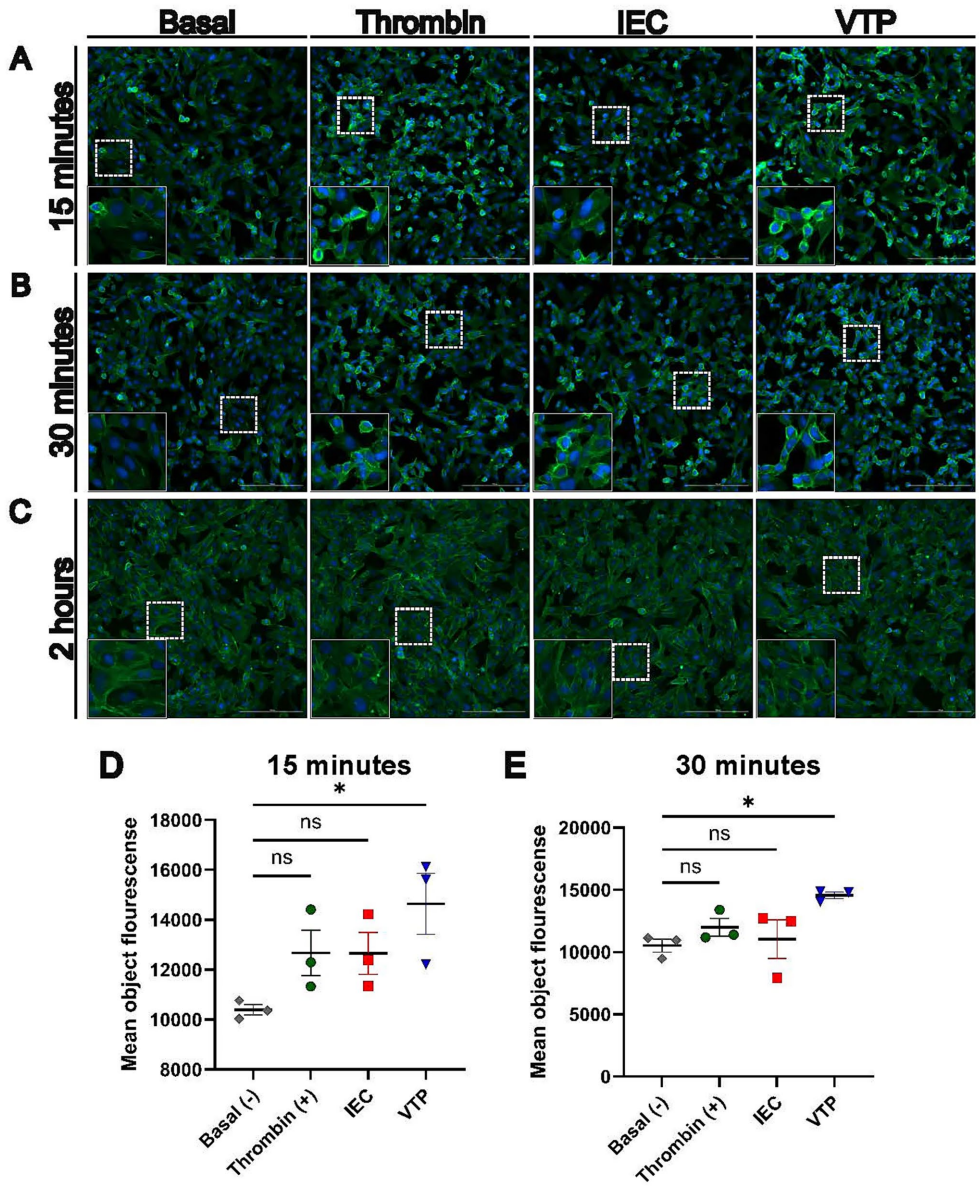

FIGURE 8
HBMECs exposed to *T. pallidum* displayed a temporal contraction of F-actin, and increased F-actin fluorescence intensity. **(A–C)** Fluorescent phalloidin F-actin (Green) staining of HBMECs exposed to basal TpCM2 media, or 10 nM bovine thrombin, infection extract control (IEC), and viable *T. pallidum* (VTP). Exposures occurred for **(A)** 15 min, **(B)** 30 min, **(C)** 2 h. HBMECs were counterstained with DAPI (Blue). Images were taken in the center of each well using a 20× objective lens. In the lower left side of each panel an inset shows a magnified region of the image, and the location of the original image used for magnification is shown by a dotted box. Scale bar represents 200 μm. **(D,E)** Plots showing image quantitation; images were taken in an automated 3 × 3 grid in the center of each well using a 20× objective lens, then stitched linearly to form a single image. Quantified mean object F-actin fluorescence intensity of HBMECs at **(D)** 15- and **(E)** 30-min of exposure. Each data point represents a biological replicate, which is defined here as an independently treated and imaged well. Significant differences were determined by one-way ANOVA followed by Dunnetts multiple comparison between each condition and the basal media-exposed condition. p-values < 0.05 were considered significant. Error bars indicate the mean with standard deviation. ns = not significant, * indicates a p-value ≤ 0.05.

(Table 4; Supplementary Table 1). Immune signaling genes downstream of both IFN and TNF, such as the NF-κB factors *TCIM* (Transcriptional and Immune Response Regulator), *NFKB1*, *NFKB2*, and *RelB*, were upregulated, while the NF-κB inhibitor *IKBKE* (Inhibitor of nuclear factor Kappa-B Kinase subunit Epsilon) was downregulated (Table 4; Supplementary Table 1). Collectively these findings indicate *T. pallidum* exposure alters TNF, IFN signaling, NF-κB signaling and the endothelial immune response to *T. pallidum*.

Endothelial cell death and viability signaling is altered during *T. pallidum* exposure

In this study, we also found cell death signaling pathways to be overrepresented in both Sigora and hallmark gene set analyses. The apoptosis hallmark gene set was downregulated at 4- and 12-h and was simultaneously up- and downregulated at 24-h, though upregulation was more significant (Figures 7B–D). Many

pro-apoptotic factors within these pathways were DE, including upregulation of pro-apoptotic genes *PMAIP1* (Phorbol-12-Myristate-13-Acetate-Induced Protein 1 [also known as Noxa]), *BBC3* (Bcl-2 Binding Component 3 [also known as Puma]), and *BCL2L11* (Bcl-2 like 11 [also known as *BIM*]), and downregulation of the anti-apoptotic factor *BCL2A1* (Table 4; Supplementary Table 1). Sigora pathway analysis identified overrepresentation of pathways related to cell death signaling through p53 at the 24-h timepoint, where DE genes involved in p53-mediated cell death include upregulation of pro-apoptotic genes *TP73* (Tumor Protein 73), and *TP53INP1* (Tumor Protein p53 Inducible Nuclear Protein 1). Finally, key apoptosis activators *CASP8* (Caspase 8) and *CASP1* were downregulated at 24-h (Table 4). These findings demonstrate the dysregulation of apoptotic signaling through intrinsic cell death pathways, such as p53, BH3-only, and through interference with CASP8-regulated cell death signaling.

Discussion

In this study we investigated the molecular landscape of *T. pallidum*-host interactions through global time-course transcriptomic analyses of HBMECs exposed to viable *T. pallidum*. A prominent transcriptional signature that was observed in this study was endothelial to mesenchymal transition (EndMT), a cellular transformation whereby endothelial cells transition across, or between, intermediary mesenchymal phenotypes (Nieto et al., 2016; Piera-Velazquez and Jimenez, 2019). Overrepresentation of EndMT pathways or hallmark gene sets, or factors that induce this response, were observed at all timepoints in the study. Further, hallmark gene sets of cellular processes involved in EndMT were overrepresented at the 24-h timepoint, namely angiogenesis and myogenesis. Consistent with these findings, endothelial markers were downregulated, while mesenchymal markers were upregulated in HBMECs exposed to *T. pallidum* (Cho et al., 2018; Piera-Velazquez and Jimenez, 2019). TF enrichment analysis, which identifies TFs that may be responsible for the observed changes in gene expression, indicated that highly connected networks of EndMT-related TFs were enriched across all timepoints. These networks include the essential EndMT-driving TF Snail (Kokudo et al., 2008; Derada Troletti et al., 2019), which was increased in expression on both the transcript and protein levels in HBMECs exposed to *T. pallidum*. Snail upregulation has been shown to promote endothelial permeability and barrier traversal of other bloodborne pathogens (Kim et al., 2015; Yang et al., 2016), and the processes of EndMT and EMT have been proposed to be critical for disrupting endothelial barrier integrity during infectious disease-induced inflammatory conditions (Hofman and Vouret-Craviari, 2012; Cho et al., 2018). In a non-infectious disease context, EndMT promotes tumor cell metastasis during, and prior to, tumor cell-endothelial engagement, facilitating invasion of tumor cells into tissues (Peinado et al., 2017). Shared mechanisms of dissemination between the metastasis of cancer cells and invasive bacteria have been proposed previously (Cameron, 2003; Lähteenmäki et al., 2005; Church et al., 2019), and it is plausible that *T. pallidum* employs convergent mechanisms to disseminate.

Fibrosis and endothelial fibrotic dysregulation, as observed in obliterative endarteritis (Carlson et al., 2011) or syphilis-induced vasculitis (Heubner's arteritis) (Holland et al., 1986; Asdaghi et al., 2007), are common manifestations of syphilis that can lead to vascular occlusion, tissue ischemia, and infarction (Carlson et al., 2011). Fibrotic dysregulation of endothelial sites (Mao et al., 2018; Corrêa et al., 2023) and retinal vasculitis/fibrosis (Mendelsohn and Jampol, 1984; Bollemeijer et al., 2016) are frequently reported during meningovascular syphilis. Endothelial phenotype modifications have also been documented, where corneal endothelial cells develop a fibroblast-like phenotype with an altered ECM composition (Kawaguchi et al., 2001). EndMT is an important contributor to vascular and fibrotic disease (Zeisberg et al., 2007; Piera-Velazquez and Jimenez, 2019), including through dysregulation of the ECM. The identification of an overarching EndMT transcriptional profile in this study supports clinical observations of endothelial fibrotic involvement during syphilis and identifies a potential functional role for EndMT in weakening cell–cell junctions, *T. pallidum* dissemination, and syphilis disease manifestations.

Pathway overrepresentation analysis revealed significant alterations in EndMT-inducing signaling pathways and hallmark gene sets, including canonical and non-canonical TGFβ, SMAD, β-catenin, NOTCH, NF-κB, and RTK pathways. Indicators of TGFβ activation that induce or potentiate EndMT (Wermuth et al., 2016; Piera-Velazquez and Jimenez, 2019; Yue et al., 2021) were upregulated, including *NOTCH1*, *IL-11*, *POSTN*, and *EDN1*. Also upregulated were *Nectin-4*, an adherens junction component that promotes EMT through β-catenin/Wnt (Noyce et al., 2011; Siddharth et al., 2017), and *TCIM* that positively regulates β-catenin, endothelial permeability, and MAPK immune signaling (Kim et al., 2009). TGFβ negative-feedback regulation, which is activated downstream of TGFβ pathway activation (Yan et al., 2018), was evident through elevated transcripts of inhibitory *SMAD7*, SMAD negative regulators *PMEPA1*, *ID1*, *ID2*, and *ID3*, and decreased transcript levels for TGFβ activators *SMAD3*, *TGFBR2*, and *TGFBR3*. In parallel, upregulation of *PDGFB*, *PGF*, and *VEGFA* indicated that growth factor activity is altered during *T. pallidum*-endothelial engagement.

The observation of TGFβ activation is consistent with a prior study showing a slight upregulation of TGFβ transcripts in skin biopsies from individuals with secondary syphilis compared to healthy controls (Cruz et al., 2012). The altered hallmark gene sets observed in the current study are also consistent with previous investigations showing that individual *T. pallidum* proteins induce EndMT-related signaling pathways within host cells. Responses include Tp1038 (TpF1) eliciting VEGF/growth-factor-like activity on human umbilical vein endothelial cells (HUVECs) (Pozzobon et al., 2016), and Tp0136 inducing fibronectin-mediated integrin-β1 signaling and subsequent microvascular endothelial cell migration (Luo et al., 2020). Immune secretion studies have also shown that HBMECs exposed to *T. pallidum* demonstrate increased VEGF secretion (Waugh et al., 2023). These findings contextualize the observation that rabbits immunized with a tri-antigen vaccine cocktail comprised of vascular adhesin Tp0751 (Kao et al., 2017) and conserved regions of select *T. pallidum* repeat (Tpr) proteins (Giacani et al., 2010) exhibit decreased TGFβ transcripts in primary chancres and reduced *T. pallidum* dissemination following *T. pallidum* challenge, compared to challenged unimmunized rabbits (Lukehart et al., 2022). Reduced TGFβ expression would dampen EndMT-promoting signaling at primary chancre sites, thereby reducing the pathology associated with inflammation and endothelial remodeling and attenuating *T. pallidum* dissemination in immunized animals.

Genes and pathways that regulate ECM organization were significantly enriched in the current study, including genes encoding the MMP, ADAM, and ADAML family of matrix proteinases. Previous investigations reported that *T. pallidum* influences the MMP/Tissue inhibitors of metalloproteinases (TIMP) equilibrium in differentiated THP-1 cells (Lin et al., 2019), and that *T. pallidum* proteins Tp0136 and Tp0574 (Tp47) alter the MMP/TIMP balance in human dermal vascular smooth muscle cells (HDVSMCs) (Cai et al., 2022) and HUVECs (Gao et al., 2019). Notably, Tp0136 was shown to alter MMP expression through the PI3K and MAPK signaling cascades (Cai et al., 2022), pathways involved in non-canonical TGFβ signaling (Piera-Velazquez and Jimenez, 2019) that were also found to be altered in the present study. These findings also support the previous report that HBMECs exposed to *T. pallidum* displayed reduced abundance of multiple ECM proteins (Waugh et al., 2023).

Reports in the literature demonstrate that integrin, ECM signaling, and Rho GTPase regulatory pathways can be exploited by invasive pathogenic bacteria to promote epithelial or endothelial barrier traversal (Popoff, 2014), whereby pathogenic bacteria utilize ECM components as bridging molecules to engage host receptors (Talay et al., 2000; Schwarz-Linek et al., 2003). Growth factor and ECM signaling are cooperative, since ECM constituents can coordinate integrin and RTK signaling (Maldonado and Hagood, 2021). In the current study, integrin interactions, ECM organization, and Rho GTPase pathways were overrepresented in HBMECs exposed to *T. pallidum*. The ability of *T. pallidum* and its constituent proteins to bind ECM components has been well-established (Cameron, 2003; Cameron et al., 2004; Brinkman et al., 2008; Kao et al., 2017; Lithgow et al., 2020; Primus et al., 2020). Previous work demonstrated that *T. pallidum* fibronectin binding proteins can signal through integrins (Luo et al., 2020), and that *T. pallidum* adherence to endothelial cells and fibronectin is reduced in the presence of peptides containing the arginine-glycine-aspartic acid (RGD) cell binding motif found in fibronectin (Lee et al., 2003). Integrins were DE in this study, including upregulation of RGD motif-binding integrin *ITGB3*, which is involved in host-pathogen signal transduction (McDonnell et al., 2016; Ludwig et al., 2021). Relatedly, we observed that *T. pallidum*-exposed HBMECs displayed increased F-actin signal intensity and a rounded morphology alongside a prominent cortical actin ring, which are hallmarks of RhoA activation (Vouret-Craviari et al., 1998). These morphological alterations occurred within 15-min of *T. pallidum* exposure, whereas cell-structure signaling pathways were first observed to be altered at 4-h. These data indicate that *T. pallidum* engagement with endothelial cells results in immediate alteration in cellular signaling, which is followed by transcriptional alteration during prolongued contact. Alternatively, transcriptional alterations may be initiated at the 45-min timepoint but not meet the fold change cut-off. Activation of RhoA downstream of *T. pallidum*-ECM interactions and subsequent enhancement of endothelial traversal has been previously proposed (Quintero et al., 2015; Waugh et al., 2023), and it has been shown that select *T. pallidum* proteins induce F-actin reorganization through Rho-associated protein kinase (ROCK)-regulated signaling in HUVECs (Zhang et al., 2014). In a similar study, human dermal lymphatic endothelial cells (HDLECs) exposed to the pathogenic spirochete *Leptospira interrogans* sv. Copenhageni displayed increased F-actin localization and intensity around the cell periphery (Sato and Coburn, 2017).

Although *RhoA* was not DE in this study, multiple Rho family members were DE, including *RhoB* and *RND1* as the most significantly upregulated. RhoB functions independently to promote endothelial permeability by decreasing cell–cell contacts, and together with RhoA induces endothelial permeability downstream of endothelial activation (Reinhard et al., 2016; Pronk et al., 2017). Increased RhoB expression also decreases VE-Cadherin localization and accumulation at cell junctions (Reinhard et al., 2016; Pronk et al., 2017). RND1, which is induced by VEGF and TGFβ (Suehiro et al., 2014; Okada et al., 2015), also disrupts adherens junctions and promotes endothelial cell rounding (Gottesbühren et al., 2012). These observations provide mechanistic insight into the prior observation that *T. pallidum* modifies endothelial VE-cadherin architecture (Lithgow et al., 2021), and highlights the modulatory effect that *T. pallidum* has on endothelial cytoskeletal and junctional signaling pathways.

The delayed-type hypersensitivity (DTH) response, which is dependent on activation of macrophages, is important for clearing local *T. pallidum* infection (Lukehart et al., 1992; Carlson et al., 2011). In the current study, we detected significant downregulation of *MCP-1* (*CCL2*), *CSF1*, *CSF2*, and *CSF3*. These observations corroborate previous findings where *T. pallidum*-exposed HBMECs displayed reduced secretion of MCP-1 and reduced protein expression of CSF1 (Waugh et al., 2023), and where activated THP-1 macrophages displayed reduced MCP-1 secretion following exposure to *T. pallidum*-derived antimicrobial peptides (Houston et al., 2022). MCP-1 and CSF proteins are critical for inducing the DTH response, as these cytokines mediate monocyte recruitment from the bloodstream to sites of endothelial inflammation (Hume et al., 1988; Gunn et al., 1997), with subsequent maturation of monocytes to activated macrophages within tissue sites. Due to the importance of DTH responses in clearing local *T. pallidum* infection (Lukehart et al., 1992; Carlson et al., 2011), reduced expression of these cytokines during *T. pallidum* contact might dampen monocyte recruitment and macrophage activity, aiding in *T. pallidum* immune avoidance and persistence. Additionally, IFN immune responses were highly overrepresented and downregulated in the dataset. Given the importance of IFN signaling in anti-viral immunity, the observed downregulation of IFN signaling upon *T. pallidum* engagement with HBMECs could provide additional context for the frequent occurrence of HIV-*T. pallidum* co-infections (Wu et al., 2021).

Symptoms stemming from endothelial, mucosal, and tissue destruction are observed at all stages of syphilis and have features characteristic of the process of necroptotic cell death (LaFond and Lukehart, 2006; Carlson et al., 2011). In the current study, apoptosis and TP53-regulated and apoptotic cell death signaling pathways were overrepresented, while necroptosis signaling pathways were not, despite a previous proteomic analysis detecting necroptosis overrepresentation when *in vivo T. pallidum* was exposed to HBMECs (Waugh et al., 2023). However, necroptosis regulatory factors were DE, including downregulation of the key necroptosis regulator *CASP8* which directs apoptotic signaling to necroptosis when inhibited (Fritsch et al., 2019). It is possible that the *in vitro T. pallidum*-endothelial cell system used in the current study lacks the full complement of factors required to induce a complete necroptotic response within endothelial cells exposed to *T. pallidum*, and confirmation of this prediction must await further studies.

Our investigations herein expand understanding of the endothelial cellular responses induced upon exposure to *T. pallidum*. However, there are limitations to our experimental

approach. This study focused on the brain microvasculature, and endothelial cells of different anatomical origin may respond differently to *T. pallidum*. Pericytes, astrocytes, and other cell types contribute to the formation and function of the endothelial and blood–brain barriers, and since the current study investigated HBMECs in monoculture, it may not be representative of the holistic response of endothelial cells to *T. pallidum in vivo*. Also, the immortalized hCMEC/d3 cell line was used for these studies, and the response of these immortalized cells may differ from those of primary endothelial cells. Further, delineating whether the endothelial responses observed are the result of a protective response raised by the host against *T. pallidum* infection, or a *T. pallidum*-induced manipulation of the host response to enhance pathogenesis of the bacterium, is not easily determined. Finally, the IEC media used in this study is an imperfect control, as it is more inflammatory than the background basal media (Waugh et al., 2023). This may account for lack of statistical significance in microscopy analyses in F-actin fluorescence intensity between the IEC and VTP treated groups, since inflammatory responses and residual *T. pallidum* components may affect endothelial cell behavior. However, due to the complex nature of the *T. pallidum* culture systems (Lukehart and Marra, 2007; Edmondson et al., 2018), this control provides the best comparator to measure cellular responses raised specifically to viable *T. pallidum*.

This study provides novel molecular insights into the global host endothelial response to *T. pallidum* and highlights the importance of the ECM for *T. pallidum* pathogenesis. Due to the importance of EMT and EndMT in fetal development and fibrotic disease (Cho et al., 2018; Piera-Velazquez and Jimenez, 2019), this study identifies the potential role of EndMT in syphilis disease manifestations observed in infectious and congenital syphilis. Indeed, our findings may further the understanding of HIV-syphilis co-infection since current and previous (Waugh et al., 2023) observations show that *T. pallidum* exposure downregulates IFN responses integral to both anti-viral immunity and macrophage-mediated clearance of *T. pallidum*. Future multi-omic and data integration investigations focused on the disease stage-specific host response to *T. pallidum*, specifically investigating systemic changes in the host transcriptome, proteome, and metabolome, will further enhance understanding of *T. pallidum*-host interactions and may provide insight into syphilis vaccine development.

Data availability statement

The datasets presented in this study can be found in online repositories. All sequencing data are archived on GEO (accession: GSE281329) and are publicly available.

Ethics statement

The animal study was approved by University of Victoria Animal Care Committee. The study was conducted in accordance with the local legislation and institutional requirements.

Author contributions

SW: Data curation, Conceptualization, Investigation, Writing – review & editing, Formal analysis, Methodology, Writing – original draft. MG: Writing – review & editing, Formal analysis. AG: Investigation, Writing – review & editing, Methodology. AR: Methodology, Writing – review & editing, Investigation. KL: Conceptualization, Writing – review & editing. RF: Writing – review & editing, Methodology. RH: Writing – review & editing, Methodology, Conceptualization. AL: Writing – review & editing, Conceptualization, Formal analysis. CC: Supervision, Formal analysis, Conceptualization, Project administration, Writing – review & editing, Writing – original draft, Funding acquisition.

Funding

The author(s) declare that financial support was received for the research and/or publication of this article. This work was supported by grants U19AI144133, U01AI18203 and the MERIT award R37AI051334 (CC) from the National Institute of Allergy and Infectious Diseases (NIAID) at the National Institutes of Health (NIH), as well as awards from Open Philanthropy (52345) and the Canadian Institutes for Health Research (CIHR; 506704 to CC and AL and 471857 to CC) and funding from CIHR Foundation grant FDN-154287 to RH. SW is the recipient of a CIHR Canada Graduate Scholarship-Doctoral (CGS-D), and MG is the recipient of a CIHR Postdoctoral Fellowship and a NIAID Developmental Research Project Award.

Acknowledgments

We would like to acknowledge Jenna Fleetwood for their assistance with this project. We would also like to acknowledge Travis Blimkie for their assistance with the GEO database. Additionally, we want to acknowledge Drs. Diane Edmondson and Steven Norris for their contribution to the field of syphilis research through the development of an *in vitro* culture system.

Conflict of interest

The authors declare that the research was conducted in the absence of any commercial or financial relationships that could be construed as a potential conflict of interest.

The author(s) declared that they were an editorial board member of Frontiers, at the time of submission. This had no impact on the peer review process and the final decision.

Generative AI statement

The authors declare that no Gen AI was used in the creation of this manuscript.

Any alternative text (alt text) provided alongside figures in this article has been generated by Frontiers with the support of artificial intelligence and reasonable efforts have been made to ensure accuracy,

including review by the authors wherever possible. If you identify any issues, please contact us.

Publisher's note

All claims expressed in this article are solely those of the authors and do not necessarily represent those of their affiliated organizations, or those of the publisher, the editors and the reviewers. Any product that may be evaluated in this article, or claim that may be made by its manufacturer, is not guaranteed or endorsed by the publisher.

Supplementary material

The Supplementary material for this article can be found online at: https://www.frontiersin.org/articles/10.3389/fmicb.2025.1649738/full#supplementary-material

References

Aho, J., Lybeck, C., Tetteh, A., Issa, C., Kouyoumdjian, F., Wong, J., et al. (2022). Rising syphilis rates in Canada, 2011–2020. *Can. Commun. Dis. Rep.* 48, 52–60. doi: 10.14745/ccdr.v48i23a01

Anders, S., Pyl, P. T., and Huber, W. (2015). HTSeq—a python framework to work with high-throughput sequencing data. *Bioinformatics* 31, 166–169. doi: 10.1093/bioinformatics/btu638

Asdaghi, N., Muayqil, T., Scozzafava, J., Jassal, R., Saqqur, M., and Jeerakathil, T. J. (2007). The re-emergence in Canada of meningovascular syphilis: 2 patients with headache and stroke. *CMAJ* 176, 1699–1700. doi: 10.1503/cmaj.070371

Blimkie, T. M., An, A., and Hancock, R. E. W. (2024). Facilitating pathway and network based analysis of RNA-Seq data with pathlinkR. *PLoS Comput. Biol.* 20:e1012422. doi: 10.1371/journal.pcbi.1012422

Bollemeijer, J. G., Wieringa, W. G., Missotten, T. O. A. R., Meenken, I., ten Dam-van Loon, N. H., Rothova, A., et al. (2016). Clinical manifestations and outcome of syphilitic uveitis. *Invest. Ophthalmol. Vis. Sci.* 57, 404–411. doi: 10.1167/iovs.15-17906

Brinkman, M. B., McGill, M. A., Pettersson, J., Rogers, A., Matějková, P., Šmajs, D., et al. (2008). A novel *Treponema pallidum* antigen, TP0136, is an outer membrane protein that binds human fibronectin. *Infect. Immun.* 76, 1848–1857. doi: 10.1128/IAI.01424-07

Cai, C.-X., Li, S.-L., Lin, H.-L., Wei, Z.-H., Xie, L., Lin, L.-R., et al. (2022). *Treponema pallidum* protein Tp0136 promoting MMPs/TIMPs imbalance via PI3K, MAPK and NF-κB signalling pathways in HDVSMCs. *Heliyon* 8:e12065. doi: 10.1016/j.heliyon.2022.e12065

Cameron, C. E. (2003). Identification of a *Treponema pallidum* laminin-binding protein. *Infect. Immun.* 71, 2525–2533. doi: 10.1128/iai.71.5.2525-2533.2003

Cameron, C. E., Brown, E. L., Kuroiwa, J. M. Y., Schnapp, L. M., and Brouwer, N. L. (2004). *Treponema pallidum* fibronectin-binding proteins. *J. Bacteriol.* 186, 7019–7022. doi: 10.1128/JB.186.20.7019-7022.2004

Carlson, J. A., Dabiri, G., Cribier, B., and Sell, S. (2011). The immunopathobiology of syphilis: the manifestations and course of syphilis are determined by the level of delayed-type hypersensitivity. *Am. J. Dermatopathol.* 33, 433–460. doi: 10.1097/DAD.0b013e3181e8b587

CDC (2024). National overview of STIs in 2023. *STI Statistics*. Available online at: https://www.cdc.gov/sti-statistics/annual/summary.html (Accessed September 15, 2025).

Chen, T., Wan, B., Wang, M., Lin, S., Wu, Y., and Huang, J. (2023). Evaluating the global, regional, and national impact of syphilis: results from the global burden of disease study 2019. *Sci. Rep.* 13:11386. doi: 10.1038/s41598-023-38294-4

Cho, J. G., Lee, A., Chang, W., Lee, M.-S., and Kim, J. (2018). Endothelial to mesenchymal transition represents a key link in the interaction between inflammation and endothelial dysfunction. *Front. Immunol.* 9:294. doi: 10.3389/fimmu.2018.00294

Church, B., Wall, E., Webb, J. R., and Cameron, C. E. (2019). Interaction of *Treponema pallidum*, the syphilis spirochete, with human platelets. *PLoS One* 14:e0210902. doi: 10.1371/journal.pone.0210902

Ciszewski, W. M., Wawro, M. E., Sacewicz-Hofman, I., and Sobierajska, K. (2021). Cytoskeleton reorganization in EndMT—the role in cancer and fibrotic diseases. *Int. J. Mol. Sci.* 22:11607. doi: 10.3390/ijms222111607

Corrêa, D. G., de Souza, S. R., de Freddi, T. A. L., Fonseca, A. P. A., dos Santos, R. Q., and Hygino da Cruz, L. C. Jr. (2023). Imaging features of neurosyphilis. *J. Neuroradiol.* 50, 241–252. doi: 10.1016/j.neurad.2023.01.003

Cruz, A. R., Ramirez, L. G., Zuluaga, A. V., Pillay, A., Abreu, C., Valencia, C. A., et al. (2012). Immune evasion and recognition of the syphilis spirochete in blood and skin of secondary syphilis patients: two immunologically distinct compartments. *PLoS Negl. Trop. Dis.* 6:e1717. doi: 10.1371/journal.pntd.0001717

Cucoranu, I., Clempus, R., Dikalova, A., Phelan, P. J., Ariyan, S., Dikalov, S., et al. (2005). NAD(P)H oxidase 4 mediates transforming growth factor-beta1-induced differentiation of cardiac fibroblasts into myofibroblasts. *Circ. Res.* 97, 900–907. doi: 10.1161/01.RES.0000187457.24338.3D

Derada Troletti, C., Fontijn, R. D., Gowing, E., Charabati, M., van Het Hof, B., Didouh, I., et al. (2019). Inflammation-induced endothelial to mesenchymal transition promotes brain endothelial cell dysfunction and occurs during multiple sclerosis pathophysiology. *Cell Death Dis.* 10, 1–13. doi: 10.1038/s41419-018-1294-2

Dobin, A., Davis, C. A., Schlesinger, F., Drenkow, J., Zaleski, C., Jha, S., et al. (2013). STAR: ultrafast universal RNA-seq aligner. *Bioinformatics* 29, 15–21. doi: 10.1093/bioinformatics/bts635

Eapen, M. S., Lu, W., Gaikwad, A. V., Bhattarai, P., Chia, C., Hardikar, A., et al. (2020). Endothelial to mesenchymal transition: a precursor to post-COVID-19 interstitial pulmonary fibrosis and vascular obliteration? *Eur. Respir. J.* 56:2003167. doi: 10.1183/13993003.03167-2020

Edmondson, D. G., Hu, B., and Norris, S. J. (2018). Long-term in vitro culture of the syphilis spirochete *Treponema pallidum* subsp. *pallidum*. *MBio*:9. doi: 10.1128/mBio.01153-18

Edmondson, D. G., and Norris, S. J. (2021). In vitro cultivation of the syphilis spirochete *Treponema pallidum*. *Curr. Protoc.* 1:e44. doi: 10.1002/cpz1.44

Elsafadi, M., Manikandan, M., Atteya, M., Abu Dawud, R., Almalki, S., Ali Kaimkhani, Z., et al. (2017). SERPINB2 is a novel TGFβ-responsive lineage fate determinant of human bone marrow stromal cells. *Sci. Rep.* 7:10797. doi: 10.1038/s41598-017-10983-x

Ewels, P., Magnusson, M., Lundin, S., and Käller, M. (2016). MultiQC: summarize analysis results for multiple tools and samples in a single report. *Bioinformatics* 32, 3047–3048. doi: 10.1093/bioinformatics/btw354

Foroushani, A. B. K., Brinkman, F. S. L., and Lynn, D. J. (2013). Pathway-GPS and SIGORA: identifying relevant pathways based on the over-representation of their gene-pair signatures. *PeerJ* 1:e229. doi: 10.7717/peerj.229

Fritsch, M., Günther, S. D., Schwarzer, R., Albert, M.-C., Schorn, F., Werthenbach, J. P., et al. (2019). Caspase-8 is the molecular switch for apoptosis, necroptosis and pyroptosis. *Nature* 575, 683–687. doi: 10.1038/s41586-019-1770-6

Gao, Z.-X., Luo, X., Liu, L.-L., Lin, L.-R., Tong, M.-L., and Yang, T.-C. (2019). Recombinant *Treponema pallidum* protein Tp47 induces angiogenesis by modulating the matrix metalloproteinase/tissue inhibitor of metalloproteinase balance in endothelial cells. *J. Eur. Acad. Dermatol. Venereol.* 33, 1958–1970. doi: 10.1111/jdv.15725

Giacani, L., Molini, B. J., Kim, E. Y., Godornes, B. C., Leader, B. T., Tantalo, L. C., et al. (2010). Antigenic variation in *Treponema pallidum*: TprK sequence diversity accumulates in response to immune pressure during experimental syphilis. *J. Immunol.* 184, 3822–3829. doi: 10.4049/jimmunol.0902788

Gillespie, M., Jassal, B., Stephan, R., Milacic, M., Rothfels, K., Senff-Ribeiro, A., et al. (2022). The reactome pathway knowledgebase 2022. *Nucleic Acids Res.* 50, D687–D692. doi: 10.1093/nar/gkab1028

Gilmour, L. S., and Walls, T. (2023). Congenital syphilis: a review of global epidemiology. *Clin. Microbiol. Rev.* 36, e00126–e00122. doi: 10.1128/cmr.00126-22

Gottesbühren, U., Garg, R., Riou, P., McColl, B., Brayson, D., and Ridley, A. J. (2012). Rnd3 induces stress fibres in endothelial cells through RhoB. *Biol. Open* 2, 210–216. doi: 10.1242/bio.20123574

Gunn, M. D., Nelken, N. A., Liao, X., and Williams, L. T. (1997). Monocyte chemoattractant protein-1 is sufficient for the chemotaxis of monocytes and lymphocytes in transgenic mice but requires an additional stimulus for inflammatory activation. *J. Immunol.* 158, 376–383. doi: 10.4049/jimmunol.158.1.376

Hofman, P., and Vouret-Craviari, V. (2012). Microbes-induced EMT at the crossroad of inflammation and cancer. *Gut Microbes* 3, 176–185. doi: 10.4161/gmic.20288

Holland, B. A., Perrett, L. V., and Mills, C. M. (1986). Meningovascular syphilis: CT and MR findings. *Radiology* 158, 439–442. doi: 10.1148/radiology.158.2.3941870

Houston, S., Schovanek, E., Conway, K. M. E., Mustafa, S., Gomez, A., Ramaswamy, R., et al. (2022). Identification and functional characterization of peptides with antimicrobial activity from the syphilis spirochete, *Treponema pallidum*. *Front. Microbiol.* 13:888525. doi: 10.3389/fmicb.2022.888525

Hume, D. A., Pavli, P., Donahue, R. E., and Fidler, I. J. (1988). The effect of human recombinant macrophage colony-stimulating factor (CSF-1) on the murine mononuclear phagocyte system in vivo. *J. Immunol.* 141, 3405–3409. doi: 10.4049/jimmunol.141.10.3405

Jin, Y., Li, F., Zheng, C., Wang, Y., Fang, Z., Guo, C., et al. (2014). NEDD9 promotes lung cancer metastasis through epithelial-mesenchymal transition. *Int. J. Cancer* 134, 2294–2304. doi: 10.1002/ijc.28568

Kao, W.-C. A., Pětrošová, H., Ebady, R., Lithgow, K. V., Rojas, P., Zhang, Y., et al. (2017). Identification of Tp0751 (pallilysin) as a *Treponema pallidum* vascular adhesin by heterologous expression in the Lyme disease spirochete. *Sci. Rep.* 7, 1–13. doi: 10.1038/s41598-017-01589-4

Kawaguchi, R., Saika, S., Wakayama, M., Ooshima, A., Ohnishi, Y., and Yabe, H. (2001). Extracellular matrix components in a case of retrocorneal membrane associated with syphilitic interstitial keratitis. *Cornea* 20, 100–103. doi: 10.1097/00003226-200101000-00019

Keenan, A. B., Torre, D., Lachmann, A., Leong, A. K., Wojciechowicz, M. L., Utti, V., et al. (2019). ChEA3: transcription factor enrichment analysis by orthogonal omics integration. *Nucleic Acids Res.* 47, W212–W224. doi: 10.1093/nar/gkz446

Kenyon, C., Osbak, K. K., Crucitti, T., and Kestens, L. (2017). The immunological response to syphilis differs by HIV status; a prospective observational cohort study. *BMC Infect. Dis.* 17:111. doi: 10.1186/s12879-017-2201-7

Kenyon, C., Tsoumanis, A., Osbak, K., Van Esbroeck, M., Florence, E., Crucitti, T., et al. (2018). Repeat syphilis has a different immune response compared with initial syphilis: an analysis of biomarker kinetics in two cohorts. *Sex. Transm. Infect.* 94, 180–186. doi: 10.1136/sextrans-2017-053312

Kim, B. J., Hancock, B. M., Bermudez, A., Cid, N. D., Reyes, E., Sorge, N. M.Van, et al. (2015). Bacterial induction of Snail1 contributes to blood-brain barrier disruption. *J. Clin. Invest.* 125, 2473–2483. doi: 10.1172/JCI74159

Kim, J., Kim, Y., Kim, H.-T., Kim, D. W., Ha, Y., Kim, J., et al. (2009). TC1(C8orf4) is a novel endothelial inflammatory regulator enhancing NF-kappaB activity. *J. Immunol.* 183, 3996–4002. doi: 10.4049/jimmunol.0900956

Knudsen, A., Benfield, T., and Kofoed, K. (2009). Cytokine expression during syphilis infection in HIV-1-infected individuals. *Sex. Transm. Dis.* 36, 300–304. doi: 10.1097/OLQ.0b013e318193ca26

Kokudo, T., Suzuki, Y., Yoshimatsu, Y., Yamazaki, T., Watabe, T., and Miyazono, K. (2008). Snail is required for TGFbeta-induced endothelial-mesenchymal transition of embryonic stem cell-derived endothelial cells. *J. Cell Sci.* 121, 3317–3324. doi: 10.1242/jcs.028282

LaFond, R. E., and Lukehart, S. A. (2006). Biological basis for syphilis. *Clin. Microbiol. Rev.* 19, 29–49. doi: 10.1128/CMR.19.1.29-49.2006

Lähteenmäki, K., Edelman, S., and Korhonen, T. K. (2005). Bacterial metastasis: the host plasminogen system in bacterial invasion. *Trends Microbiol.* 13, 79–85. doi: 10.1016/j.tim.2004.12.003

Lee, J. H., Choi, H. J., Jung, J., Lee, M. G., Lee, J. B., and Lee, K. H. (2003). Receptors for *Treponema pallidum* attachment to the surface and matrix proteins of cultured human dermal microvascular endothelial cells. *Yonsei Med. J.* 44, 371–378. doi: 10.3349/ymj.2003.44.3.371

Li, H., Chang, H.-M., Lin, Y.-M., Shi, Z., and Leung, P. C. K. (2021). TGF-β1 inhibits microvascular-like formation by decreasing VCAM1 and ICAM1 via the upregulation of SNAIL in human granulosa cells. *Mol. Cell. Endocrinol.* 535:111395. doi: 10.1016/j.mce.2021.111395

Liberzon, A., Birger, C., Thorvaldsdóttir, H., Ghandi, M., Mesirov, J. P., and Tamayo, P. (2015). The molecular signatures database (MSigDB) hallmark gene set collection. *Cell Syst.* 1, 417–425. doi: 10.1016/j.cels.2015.12.004

Lin, S.-W., Gao, Z.-X., Lin, L.-R., Luo, X., Liu, L.-L., and Yang, T.-C. (2019). *Treponema pallidum* enhances human monocyte migration and invasion by dysregulating the MMP/TIMP balance. *Int. Immunopharmacol.* 75:105744. doi: 10.1016/j.intimp.2019.105744

Lithgow, K. V., Church, B., Gomez, A., Tsao, E., Houston, S., Swayne, L. A., et al. (2020). Identification of the neuroinvasive pathogen host target, LamR, as an endothelial receptor for the *Treponema pallidum* adhesin Tp0751. *mSphere* 5, e00195–e00120. doi: 10.1128/mSphere.00195-20

Lithgow, K. V., Tsao, E., Schovanek, E., Gomez, A., Swayne, L. A., and Cameron, C. E. (2021). *Treponema pallidum* disrupts VE-cadherin intercellular junctions and traverses endothelial barriers using a cholesterol-dependent mechanism. *Front. Microbiol.* 12:1790. doi: 10.3389/fmicb.2021.691731

Love, M. I., Huber, W., and Anders, S. (2014). Moderated estimation of fold change and dispersion for RNA-seq data with DESeq2. *Genome Biol.* 15:550. doi: 10.1186/s13059-014-0550-8

Ludwig, B. S., Kessler, H., Kossatz, S., and Reuning, U. (2021). RGD-binding integrins revisited: how recently discovered functions and novel synthetic ligands (re-)shape an ever-evolving field. *Cancers (Basel)* 13:1711. doi: 10.3390/cancers13071711

Lukehart, S. A., and Marra, C. M. (2007). Isolation and laboratory maintenance of *Treponema pallidum*. *Curr. Protoc. Microbiol.* Chapter 12:Unit 12A.1. doi: 10.1002/9780471729259.mc12a01s7

Lukehart, S. A., Molini, B., Gomez, A., Godornes, C., Hof, R., Fernandez, M. C., et al. (2022). Immunization with a tri-antigen syphilis vaccine significantly attenuates chancre development, reduces bacterial load, and inhibits dissemination of *Treponema pallidum*. *Vaccine* 40, 7676–7692. doi: 10.1016/j.vaccine.2022.11.002

Lukehart, S. A., Shaffer, J. M., and Baker-Zander, S. A. (1992). A subpopulation of *Treponema pallidum* is resistant to phagocytosis: possible mechanism of persistence. *J. Infect. Dis.* 166, 1449–1453. doi: 10.1093/infdis/166.6.1449

Luo, X., Lin, S.-W., Xu, Q.-Y., Ke, W.-J., Gao, Z.-X., Tong, M.-L., et al. (2020). Tp0136 targets fibronectin (RGD)/integrin β1 interactions promoting human microvascular endothelial cell migration. *Exp. Cell Res.* 396:112289. doi: 10.1016/j.yexcr.2020.112289

Ma, J., van der Zon, G., Gonçalves, M. A. F. V., van Dinther, M., Thorikay, M., Sanchez-Duffhues, G., et al. (2021). TGF-β-induced endothelial to mesenchymal transition is determined by a balance between SNAIL and ID factors. *Front. Cell Dev. Biol.* 9:616610. doi: 10.3389/fcell.2021.616610

Maldonado, H., and Hagood, J. S. (2021). Cooperative signaling between integrins and growth factor receptors in fibrosis. *J. Mol. Med.* 99, 213–224. doi: 10.1007/s00109-020-02026-2

Mao, C., Gao, J., Jin, L., Peng, B., and Guo, Y. (2018). Postmortem histopathologic analysis of neurosyphilis: a report of 3 cases with clinicopathologic correlations. *J. Neuropathol. Exp. Neurol.* 77, 296–301. doi: 10.1093/jnen/nly004

McDonnell, C. J., Garciarena, C. D., Watkin, R. L., McHale, T. M., McLoughlin, A., Claes, J., et al. (2016). Inhibition of major integrin αV β3 reduces *Staphylococcus aureus* attachment to sheared human endothelial cells. *J. Thromb. Haemost.* 14, 2536–2547. doi: 10.1111/jth.13501

Mendelsohn, A. D., and Jampol, L. M. (1984). Syphilitic retinitis. A cause of necrotizing retinitis. *Retina* 4, 221–224. doi: 10.1097/00006982-198400440-00002

Milara, J., Roger, I., Montero, P., Artigues, E., Escrivá, J., and Cortijo, J. (2022). IL-11 system participates in pulmonary artery remodeling and hypertension in pulmonary fibrosis. *Respir. Res.* 23:313. doi: 10.1186/s12931-022-02241-0

Nakerakanti, S. S., Bujor, A. M., and Trojanowska, M. (2011). CCN2 is required for the TGF-β induced activation of Smad1 – Erk1/2 signaling network. *PLoS One* 6:e21911. doi: 10.1371/journal.pone.0021911

Nieto, M. A., Huang, R. Y.-J., Jackson, R. A., and Thiery, J. P. (2016). EMT: 2016. *Cell* 166, 21–45. doi: 10.1016/j.cell.2016.06.028

Noyce, R. S., Bondre, D. G., Ha, M. N., Lin, L.-T., Sisson, G., Tsao, M.-S., et al. (2011). Tumor cell marker PVRL4 (Nectin 4) is an epithelial cell receptor for measles virus. *PLoS Pathog.* 7:e1002240. doi: 10.1371/journal.ppat.1002240

Nueda, M. J., Tarazona, S., and Conesa, A. (2014). Next maSigPro: updating maSigPro bioconductor package for RNA-seq time series. *Bioinformatics* 30, 2598–2602. doi: 10.1093/bioinformatics/btu333

Okada, T., Sinha, S., Esposito, I., Schiavon, G., López-Lago, M. A., Su, W., et al. (2015). The rho-GTPase Rnd1 suppresses mammary tumorigenesis and EMT by restraining Ras-MAPK signaling. *Nat. Cell Biol.* 17, 81–94. doi: 10.1038/ncb3082

Peinado, H., Zhang, H., Matei, I. R., Costa-Silva, B., Hoshino, A., Rodrigues, G., et al. (2017). Pre-metastatic niches: organ-specific homes for metastases. *Nat. Rev. Cancer* 17, 302–317. doi: 10.1038/nrc.2017.6

Piera-Velazquez, S., and Jimenez, S. A. (2019). Endothelial to mesenchymal transition: role in physiology and in the pathogenesis of human diseases. *Physiol. Rev.* 99, 1281–1324. doi: 10.1152/physrev.00021.2018

Pinto, M. T., Ferreira Melo, F. U., Malta, T. M., Rodrigues, E. S., Plaça, J. R., Silva, W. A., et al. (2018). Endothelial cells from different anatomical origin have distinct responses during SNAIL/TGF-β2-mediated endothelial-mesenchymal transition. *Am. J. Transl. Res.* 10, 4065–4081

Popoff, M. R. (2014). Bacterial factors exploit eukaryotic rho GTPase signaling cascades to promote invasion and proliferation within their host. *Small GTPases* 5:e28209. doi: 10.4161/sgtp.28209

Pozzobon, T., Facchinello, N., Bossi, F., Capitani, N., Benagiano, M., Di Benedetto, G., et al. (2016). *Treponema pallidum* (syphilis) antigen TpF1 induces angiogenesis through the activation of the IL-8 pathway. *Sci. Rep.* 6:18785. doi: 10.1038/srep18785

Primus, S., Rocha, S. C., Giacani, L., and Parveen, N. (2020). Identification and functional assessment of the first placental adhesin of *Treponema pallidum* that may play critical role in congenital syphilis. *Front. Microbiol.* 11:621654. doi: 10.3389/fmicb.2020.621654

Pronk, M. C. A., van Bezu, J. S. M., van Nieuw Amerongen, G. P., van Hinsbergh, V. W. M., and Hordijk, P. L. (2017). RhoA, RhoB and RhoC differentially regulate endothelial barrier function. *Small GTPases* 10:466. doi: 10.1080/21541248.2017.1339767

Quintero, C. A., Tudela, J. G., and Damiani, M. T. (2015). Rho GTPases as pathogen targets: focus on curable sexually transmitted infections. *Small GTPases* 6, 108–118. doi: 10.4161/21541248.2014.991233

Randi, A. M., and Laffan, M. A. (2017). Von Willebrand factor and angiogenesis: basic and applied issues. *J. Thromb. Haemost.* 15, 13–20. doi: 10.1111/jth.13551

Reid, T. B., Godornes, C., Campbell, V. L., Laing, K. J., Tantalo, L. C., Gomez, A., et al. (2024). *Treponema pallidum* periplasmic and membrane proteins are recognized by circulating and skin CD4+ T cells. *J. Infect. Dis.* 230, 281–292. doi: 10.1093/infdis/jiae245

Reinhard, N. R., van Helden, S. F., Anthony, E. C., Yin, T., Wu, Y. I., Goedhart, J., et al. (2016). Spatiotemporal analysis of RhoA/B/C activation in primary human endothelial cells. *Sci. Rep.* 6:25502. doi: 10.1038/srep25502

Riley, B. S., Oppenheimer-Marks, N., Hansen, E. J., Radolf, J. D., and Norgard, M. V. (1992). Virulent *Treponema pallidum* activates human vascular endothelial cells. *J. Infect. Dis.* 165, 484–493. doi: 10.1093/infdis/165.3.484

Saito, A. (2013). EMT and EndMT: regulated in similar ways? *J. Biochem.* 153, 493–495. doi: 10.1093/jb/mvt032

Samarakoon, R., Higgins, S. P., Higgins, C. E., and Higgins, P. J. (2008). TGF-β1-induced plasminogen activator inhibitor-1 expression in vascular smooth muscle cells requires pp60c-src/EGFRY845 and rho/ROCK signaling. *J. Mol. Cell. Cardiol.* 44, 527–538. doi: 10.1016/j.yjmcc.2007.12.006

Sato, H., and Coburn, J. (2017). *Leptospira interrogans* causes quantitative and morphological disturbances in adherens junctions and other biological groups of proteins in human endothelial cells. *PLoS Negl. Trop. Dis.* 11:e0005830. doi: 10.1371/journal.pntd.0005830

Schafer, S., Viswanathan, S., Widjaja, A. A., Lim, W.-W., Moreno-Moral, A., DeLaughter, D. M., et al. (2017). IL-11 is a crucial determinant of cardiovascular fibrosis. *Nature* 552, 110–115. doi: 10.1038/nature24676

Schwarz-Linek, U., Werner, J. M., Pickford, A. R., Gurusiddappa, S., Kim, J. H., Pilka, E. S., et al. (2003). Pathogenic bacteria attach to human fibronectin through a tandem beta-zipper. *Nature* 423, 177–181. doi: 10.1038/nature01589

Siddharth, S., Goutam, K., Das, S., Nayak, A., Nayak, D., Sethy, C., et al. (2017). Nectin-4 is a breast cancer stem cell marker that induces WNT/β-catenin signaling via Pi3k/Akt axis. *Int. J. Biochem. Cell Biol.* 89, 85–94. doi: 10.1016/j.biocel.2017.06.007

Spiteri, G., Unemo, M., Mårdh, O., and Amato-Gauci, A. J. (2019). The resurgence of syphilis in high-income countries in the 2000s: a focus on Europe. *Epidemiol. Infect.* 147:e143. doi: 10.1017/S0950268819000281

Suehiro, J., Kanki, Y., Makihara, C., Schadler, K., Miura, M., Manabe, Y., et al. (2014). Genome-wide approaches reveal functional vascular endothelial growth factor (VEGF)-inducible nuclear factor of activated T cells (NFAT) c1 binding to angiogenesis-related genes in the endothelium. *J. Biol. Chem.* 289, 29044–29059. doi: 10.1074/jbc.M114.555235

Talay, S. R., Zock, A., Rohde, M., Molinari, G., Oggioni, M., Pozzi, G., et al. (2000). Co-operative binding of human fibronectin to Sfbl protein triggers streptococcal invasion into respiratory epithelial cells. *Cell. Microbiol.* 2, 521–535. doi: 10.1046/j.1462-5822.2000.00076.x

Vouret-Craviari, V., Boquet, P., Pouysségur, J., and Van Obberghen-Schilling, E. (1998). Regulation of the actin cytoskeleton by thrombin in human endothelial cells: role of rho proteins in endothelial barrier function. *MBoC* 9, 2639–2653. doi: 10.1091/mbc.9.9.2639

Walsh, L. A., Nawshad, A., and Medici, D. (2011). Discoidin domain receptor 2 is a critical regulator of epithelial-mesenchymal transition. *Matrix Biol.* 30, 243–247. doi: 10.1016/j.matbio.2011.03.007

Watanabe, Y., Itoh, S., Goto, T., Ohnishi, E., Inamitsu, M., Itoh, F., et al. (2010). TMEPAI, a transmembrane TGF-β-inducible protein, sequesters smad proteins from active participation in TGF-β signaling. *Mol. Cell* 37, 123–134. doi: 10.1016/j.molcel.2009.10.028

Waugh, S., Ranasinghe, A., Gomez, A., Houston, S., Lithgow, K. V., Eshghi, A., et al. (2023). Syphilis and the host: multi-omic analysis of host cellular responses to *Treponema pallidum* provides novel insight into syphilis pathogenesis. *Front. Microbiol.* 14:1254342. doi: 10.3389/fmicb.2023.1254342

Wermuth, P. J., Li, Z., Mendoza, F. A., and Jimenez, S. A. (2016). Stimulation of transforming growth factor-β1-induced endothelial-to-mesenchymal transition and tissue fibrosis by Endothelin-1 (ET-1): a novel profibrotic effect of ET-1. *PLoS One* 11:e0161988. doi: 10.1371/journal.pone.0161988

World Health Organization (2024). Implementing the global health sector strategies on HIV, viral hepatitis and sexually transmitted infections, 2022–2030 |report on progress and gaps 2024. Available online at: https://www.who.int/publications/i/item/9789240094925 (Accessed September 5, 2024).

Wu, M. Y., Gong, H. Z., Hu, K. R., Zheng, H., Wan, X., and Li, J. (2021). Effect of syphilis infection on HIV acquisition: a systematic review and meta-analysis. *Sex. Transm. Infect.* 97, 525–533. doi: 10.1136/sextrans-2020-054706

Yan, X., and Chen, Y.-G. (2011). Smad7: not only a regulator, but also a cross-talk mediator of TGF-β signalling. *Biochem. J.* 434, 1–10. doi: 10.1042/BJ20101827

Yan, X., Xiong, X., and Chen, Y.-G. (2018). Feedback regulation of TGF-β signaling. *Acta Biochim. Biophy. Sin.* 50, 37–50. doi: 10.1093/abbs/gmx129

Yang, R., Liu, W., Miao, L., Yang, X., Fu, J., Dou, B., et al. (2016). Induction of VEGFA and Snail-1 by meningitic *Escherichia coli* mediates disruption of the blood-brain barrier. *Oncotarget* 7, 63839–63855. doi: 10.18632/oncotarget.11696

Yu, G., Wang, L.-G., Han, Y., and He, Q.-Y. (2012). clusterProfiler: an R package for comparing biological themes among gene clusters. *OMICS* 16, 284–287. doi: 10.1089/omi.2011.0118

Yue, H., Li, W., Chen, R., Wang, J., Lu, X., and Li, J. (2021). Stromal POSTN induced by TGF-β1 facilitates the migration and invasion of ovarian cancer. *Gynecol. Oncol.* 160, 530–538. doi: 10.1016/j.ygyno.2020.11.026

Zeisberg, E. M., Tarnavski, O., Zeisberg, M., Dorfman, A. L., McMullen, J. R., Gustafsson, E., et al. (2007). Endothelial-to-mesenchymal transition contributes to cardiac fibrosis. *Nat. Med.* 13, 952–961. doi: 10.1038/nm1613

Zhang, R.-L., and Wang, Q.-Q. (2020). The *Treponema pallidum* outer membrane protein Tp92 activates endothelial cells via the chemerin/CMKLR1 pathway. *Int. J. Med. Microbiol.* 310:151416. doi: 10.1016/j.ijmm.2020.151416

Zhang, R.-L., Zhang, J.-P., and Wang, Q.-Q. (2014). Recombinant *Treponema pallidum* protein Tp0965 activates endothelial cells and increases the permeability of endothelial cell monolayer. *PLoS One* 9:e115134. doi: 10.1371/journal.pone.0115134